Widespread Megaripple Activity Across the North Polar Ergs of Mars

Matthew Chojnacki[1], David Alegre Vaz[2], Simone Silvestro[3], and David C.A. Silva[4]

[1]Planetary Science Institute
[2]Centre for Earth and Space Research of the University of Coimbra
[3]INAF
[4]Centre for Earth and Space Research of the University of Coimbra

November 21, 2022

Abstract

The most expansive dune fields on Mars surround the northern polar cap where various aeolian bedform classes are modified by wind and ice. The morphology and dynamics of these ripples, intermediate-scale bedforms (termed megaripples and transverse aeolian ridges (TARs)), and sand dunes reflect information regarding regional boundary conditions. We found that populations of polar megaripples and larger TARs are distinct in terms of their morphology, spatial distribution, and mobility. Whereas regionally-restricted TARs appeared degraded and static in long-baseline observations, polar megaripples were not only widespread but migrating at relatively high rates (0.13± 0.03 m/yr) and possibly more active than other regions on Mars. This high level of activity is somewhat surprising since there is limited seasonality for aeolian transport due to surficial frost and ice during the latter half of the martian year. A comprehensive analysis of an Olympia Cavi dune field estimated that the advancement of megaripples, ripples, and dunes avalanches accounted for ~1%, ~10%, and ~100%, respectively, of the total aeolian system's sand fluxes. This included dark-toned ripples that migrated the average equivalent of 9.6±6 m/yr over just 22 days in northern summer - unprecedented rates for Mars. While bedform transport rates are some of the highest yet reported on Mars, the sand flux contribution between the different bedforms does not substantially vary from equatorial sites with lower rates. Seasonal off-cap sublimation winds and summer-time polar storms are attributed as the cause for the elevated activity, rather than cryospheric processes.

Hosted file

s7_lpsc_burriedbuzzel.gif available at https://authorea.com/users/530547/articles/597385-widespread-megaripple-activity-across-the-north-polar-ergs-of-mars

Hosted file

s3_bedrockbuzzel.gif available at https://authorea.com/users/530547/articles/597385-widespread-megaripple-activity-across-the-north-polar-ergs-of-mars

Hosted file

s2_animated_red_001374-054013_2650_ulx19621_uly37886_b.gif available at https://authorea.com/users/530547/articles/597385-widespread-megaripple-activity-across-the-north-polar-ergs-of-mars

Hosted file

s5_2798+809_west_abalos_scopuli_untitled_009433_053805_2610.gif available at https://authorea.com/users/530547/articles/597385-widespread-megaripple-activity-across-the-north-polar-ergs-of-mars

Widespread Megaripple Activity Across the North Polar Ergs of Mars

Matthew Chojnacki[*1], David A. Vaz[2], Simone Silvestro[3,4], and & David C.A. Silva[2].

Manuscript for Submission to **Journal of Geophysical Research – Planets**

[1]Planetary Science Institute, Lakewood, CO, USA.

[2]Centre for Earth and Space Research of the University of Coimbra, Observatório Geofísico e Astronómico da Universidade de Coimbra, Coimbra, Portugal.

[3]SETI Institute, Carl Sagan Center, Mountain View, CA, USA.

[4]INAF Osservatorio Astronomico di Capodimonte, Napoli, Italia.

*Corresponding Author:
Matthew Chojnacki
Planetary Science Institute,
1546 Cole Blvd #120, Lakewood, CO 80401
email:mchojnacki@psi.edu
phone: 720-961-4590

Key Points:

- Abundant megaripple populations were identified across the north polar ergs of Mars and found to be migrating with dunes and ripples.
- Polar megaripple dynamics and sand fluxes are enhanced relative to lower-latitude sites, despite the shorter migration season due to ice.
- Seasonal sublimation winds and polar storms were attributed as the cause for the elevated activity rather than cryospheric processes.

Descriptive headings for each section:

1. Introduction and motivation – introduction and motivation for the study, including a broad overview of aeolian bedforms.

2. Study region – a brief description of the north polar region and details regarding its past and current geology.

3. Overview of data sets and methods – details for our methodology and stated objectives.

4. Results – a description of results related for objectives 1-3: survey of polar megaripple occurrence, assessment of polar megaripple activity, and polar megaripple fluxes and comparisons to other bedforms.

5. Discussion – an examination on the spatial heterogeneity of polar intermediate-scale bedforms and the implications of the polar seasonal cycle on aeolian sand fluxes.

6. Conclusions: a summary of results and their possible implications.

ABSTRACT

The most expansive dune fields on Mars surround the northern polar cap where various aeolian bedform classes are modified by wind and ice. The morphology and dynamics of these ripples, intermediate-scale bedforms (termed megaripples and transverse aeolian ridges (TARs)), and sand dunes reflect information regarding regional boundary conditions. We found that populations of polar megaripples and larger TARs are distinct in terms of their morphology, spatial distribution, and mobility. Whereas regionally-restricted TARs appeared degraded and static in long-baseline observations, polar megaripples were not only widespread but migrating at relatively high rates (0.13± 0.03 m/yr) and possibly more active than other regions on Mars. This high level of activity is somewhat surprising since there is limited seasonality for aeolian transport due to surficial frost and ice during the latter half of the martian year. A comprehensive analysis of an Olympia Cavi dune field estimated that the advancement of megaripples, ripples, and dunes avalanches accounted for ~1%, ~10%, and ~100%, respectively, of the total aeolian system's sand fluxes. This included dark-toned ripples that migrated the average equivalent of 9.6±6 m/yr over just 22 days in northern summer – unprecedented rates for Mars. While bedform transport rates are some of the highest yet reported on Mars, the sand flux contribution between the different bedforms does not substantially vary from equatorial sites with lower rates. Seasonal off-cap sublimation winds and summer-time polar storms are attributed as the cause for the elevated activity, rather than cryospheric processes.

Plain Language Summary

"Megaripples" are distinct wind-driven bedforms that occur on the surface of Earth and Mars, often with sizes between that of smaller ripples and larger dunes. Recent work has found the thin martian atmosphere is capable of mobilizing some coarse-grained megaripples, overturning prior notions that these were static relic landforms from a past climate. We mapped megaripples and adjacent bedforms across the north polar sand seas, the most expansive collection of dune fields on Mars. Megaripples were found to be widespread across the region and migrating at relatively high rates relative to other sites on Mars that are at lower latitudes. This enhanced activity is likely related to the greater sand fluxes found for neighboring dunes which are driven by summer-time seasonal winds when polar ice is sublimating.

1.0 Introduction and motivation

Dune fields across Earth and Mars host a variety of aeolian bedform classes (e.g., ripples, megaripples, dunes) that vary in terms of size and particle size distribution (Bagnold, 1941; Wilson, 1973; Greeley and Iversen, 1985). Planetary bedform types include sand dunes, decimeter-wavelength impact ripples, and the generally larger ripple class of coarse-grained "megaripples" (Greeley et al., 1992; Malin and Edgett, 2001; Sullivan et al., 2005, 2008; Lancaster, 2009). Martian dark-toned, decameter-wavelength ripples are an exception, with no counterpart in terrestrial eolian environments (Vaz et al., 2017). The last several decades of Mars exploration and the arrival of high resolution orbital imaging and surface rovers have also revealed some of these bedform classes are migrating under the current climate (Sullivan et al., 2005; Silvestro et al., 2010, 2020; Chojnacki et al., 2015). Ultimately the presence and activity of a given bedform class reflects differences in their boundary conditions (e.g., grain size, wind energy, sediment supply) (Kocurek and Ewing, 2012; Chojnacki et al., 2019). For example, terrestrial megaripples that are often partially sourced by an abundant coarse sand population may rarely migrate except for very strong storm events (Sakamoto-Arnold, 1981a; Isenberg et al., 2011a).

The smallest bedform class observed from orbit on Mars (1-5 m spacing and ~40 cm tall) are dark-toned ripples (DTRs) found migrating atop dunes or within isolated patches (Bridges et al., 2011; Lapotre et al., 2016, 2018; Sullivan and Kok, 2017). The larger (10-100 m spacing and 1-14 m tall), light-toned Transverse Aeolian Ridges (TARs) can occur in association with dunes or as large TAR fields, but often lack unambiguous signs of activity (Balme et al., 2008; Geissler and Wilgus, 2017; Berman et al., 2018). The size range in between these commonly cited bedform populations (5-40 m spacing, ~1-2 m tall) have been largely unexplored and generally assumed to be inactive like TARs (Chojnacki et al., 2018). We term these intermediate-scale bedforms as "megaripples" based on their greater dimensions and brighter crests than DTRs (**Fig. 1**), where we infer the latter is due to a coarser grain size component (Greeley and Iversen, 1985). It is noted that granulometrical analysis, which is required to properly distinguish between unimodal and bimodal sand of a given bedform (Greeley and Iversen, 1985; Sullivan et al., 2008; Yizhaq et al., 2012), is unavailable for most locations on Mars.

Recent analysis using images acquired by the High Resolution Imaging Science Experiment (HiRISE) camera (0.25–1 m/pix) (McEwen et al., 2007) have shown certain locations

78 host migrating megaripples, which are most apparent among high flux dunes (Chojnacki et al.,

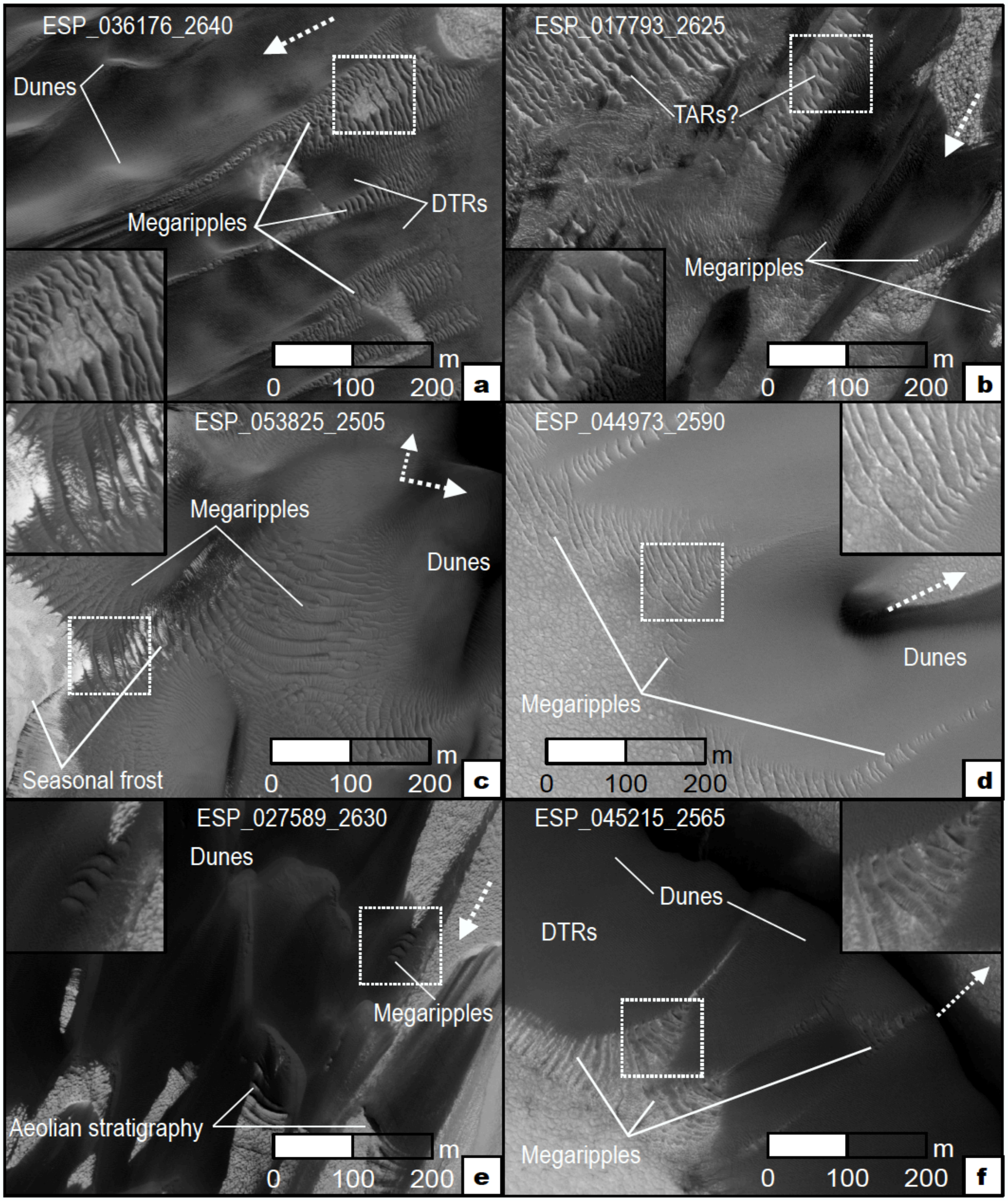

Fig. 1. (a-f) Polar bedform sites with active megaripples, as viewed in HiRISE at the same scale. Approximate transport directions (dashed arrows) are shown. Insets are 100-m-wide. All images are oriented North up unless otherwise indicated. (a) High flux bedforms in the Olympia Cavi dune field termed "Buzzel". (b) Polar bedforms that resemble TARs, alongside DTRs and megaripples. (c) Loath crater megaripples, some partially restricted by late season frost and possible intergranular ice. (d) Bright, thin megaripples found to be active in Scandi Cavi. (e) Modern bedforms that migrate over aeolian stratigraphy described by Brothers and Kocurek (2018). (f) Megaripples arranged upwind and flanking inter-erg mega-dunes.

2019; Silvestro et al., 2020). However, it is not clear how frequent this mobility is or even their broader occurrence. In particular, the northern polar latitudes of Mars has been found to have extensive migration of DTRs and dunes (Hansen et al., 2011; Bridges et al., 2011; Chojnacki et al., 2019; Fenton et al., 2021), but also has been cited to lack intermediate-scale bedforms of megaripples or TARs (Wilson and Zimbelman, 2004; Balme et al., 2008). Additionally, this effort seeks to constrain the sand flux contributions of megaripples relative to other polar bedforms.

The goal of this project is to better understand the intriguing bedform class of megaripples in one of the most complex planetary aeolian systems, namely the north circumpolar ergs. Objectives here are to 1) survey aeolian sites across the north pole of Mars for the presence of intermediate-scale bedforms, 2) assess megaripple and TAR dynamics and evaluate if any activity is restricted to certain areas or is widespread across polar sites, and 3) quantify relative sand flux contributions of polar megaripples related to other bedforms. All of the objective results will be viewed in the context of the polar environment and how regional boundary conditions impact bedform mobility across the erg. In this way, we hope to better understand polar aeolian processes, identify any seasonal effects, and quantify landscape evolution in one of the most active regions on Mars.

2.0 Study Region

The north polar region of Mars displays a range of seasonal and annual atmospheric and surface processes that continually reshape the local landscape (Smith et al., 2018). These processes are linked to the volatile and dust exchange between polar and nonpolar reservoirs, where the north polar cap is composed of seasonal CO_2 ice, residual H_2O ice, and dust (Langevin, 2005; Khayat et al., 2019). This surface-atmospheric exchange is known to drive various aeolian phenomena, such as wind streaks (Howard, 2000), seasonal and inter-annual albedo variations (Calvin et al., 2015), spiral trough evolution (Smith and Holt, 2010), dust storms (Wang and Fisher, 2009) and bedform migration (Bourke et al., 2008; Bridges et al., 2011). Expansive dune systems nearest the north polar layered deposits (NPLD) and residual cap (Hayward, 2011; Fenton, 2020) are primarily driven by Coriolis force deflected katabatic (downslope) winds from the northeast descending into a series of reentrant chasms. Indeed, sand pathways sourced from the NPLD's Planum Boreum cavi and Rupes units are most evident in Chasma Boreale, Olympia Cavi, and other reentrants that spiral southward to merge with the main erg (**Fig. 2**)(Fishbaugh and Head, 2005; Tanaka et al., 2008). The high level of bedform migration is despite the limited sediment availability caused by autumn/winter CO_2/H_2O ice accumulation that restricts saltation for most of the year (Chojnacki et al., 2019). Dune sand becomes ice-cemented while winter-time CO_2 ice buries dunes and then slowly sublimes through the Northern spring/summer until bedforms are "frost free" and mobile by summer (Ewing et al., 2010; Hansen et al., 2011). Some ice-cemented bedforms do not appear to regain mobility and were deposited into the geologic record as evidenced by the exposed aeolian cross-strata (Brothers and Kocurek, 2018).

3.0 Overview of Approach Data Sets and Methods

For the objective 1 survey we assessed bedform morphology using HiRISE images (0.25–1 m/pix) acquired in northern summer and criteria described in section 4.1. Objective 2 and 3's assessment of bedform activity relied on long-baseline (4-7 Mars years)

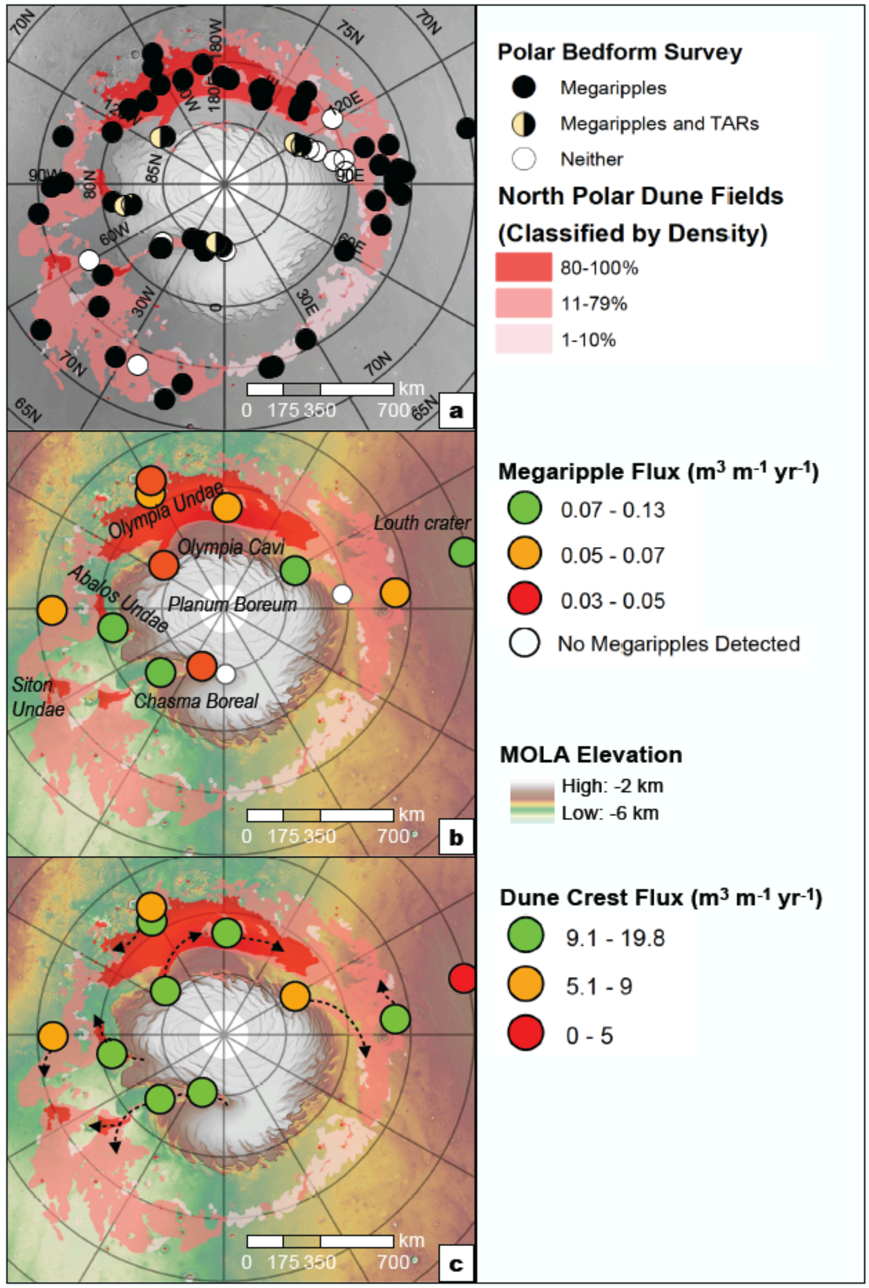

Figure 2. Polar bedform occurrence and activity results. Dune field distribution are shown in red (Hayward et al., 2014; Fenton, 2020). Base maps are MOLA shaded relief with gray-scale or colorized elevation. (a) Survey results showing HiRISE locations of dune fields with megaripples, TAR-candidates, or sites lacking either intermediate-scale bedform class. See Table S2. (b) Results showing megaripple fluxes (colored circles) from manual mapping along with two sites lacking megaripples (white circles; Fig. S1). (c) Prior results showing sand dune fluxes at the same locations (colored circles; Chojnacki et al. 2019) and simplified transport directions (dashed arrows).

orthoimages of sites with prior HiRISE Digital Terrain Models (DTMs) (1 m/post) (Chojnacki et al., 2019). Orthorectification was caried out using SOCET SET® BAE system photogrammetry software (Kirk et al., 2008), where image pairs for change detection were typically acquired within 20° of solar longitude (L_s), but in different Mars years (see Supplementary Materials (SM) section 1 for more details). Activity was quantified by mapping 3 or more consecutive megaripple crests (per area) in both the Time 1 (T1) and T2 images (**Table S1**) using ArcGIS® or QGIS. Wavelength (wr) and migration rate (m/Earth-year) were calculated using QGIS software and in-house code which ingests manually mapped crest lines from different images. Wavelength measurements correspond to the average spacing computed along transects orthogonal to the bedform traces, while migration rates were quantified assuming a local bi-orthogonal migration trend between mapped crest lines (Silvestro et al., 2020). Bedform half heights (hr), and ultimately megaripple flux estimates, were derived using the following relationship (Bridges et al., 2012);

(1) hr=wr/20

Objective 3's quantification of whole dune field fluxes required multiple approaches applied to an Olympia Cavi reentrant aeolian site (232.9°E; 84.0°N) termed here as "Buzzel" (see Diniega et al. (2017)). This site was chosen due to the abundance of adequate data and known activity (Diniega et al., 2017; Chojnacki et al., 2019). Dune front advancements were recorded with the tracing of lee fronts in ArcMap® on the T1 and T2 images, allowing migration rates and directions to be semiautomatically computed. This process integrates data derived from HiRISE orthoimages and DTMs, generating continuous measurements of migration and heights along the slip faces (Urso et al., 2018). Migration vectors were then converted to volumetric sand fluxes (*q*) ($m^3\ m^{-1}\ yr^{-1}$) by multiplying the migration rates to the dune slip face heights. Instead of reporting peak fluxes (multiplying the maximum height by the average migration, like in Urso et al. (2018)) we compute mean and median fluxes by multiplying the two variable parameters along the slip faces. This generates lower average fluxes, yet it is a more accurate representation of the overall fluxes (the same approach was followed in the flux comparison presented by Silvestro et al., 2020). Ripple and megaripple displacements were quantified for the Buzzel site using "Co-registration of Optically Sensed Images and Correlation" (COSI-Corr) software (Leprince et al., 2007) which produces a dense vectorial map of ripple migration (Bridges et al., 2012; Vaz et al., 2017). The rapid migration rates of DTRs required early summer images (Mars Year (MY) 35, L_s 95-105°), whereas MY 30 and 35 images were used to assess slower megaripples. Fluxes were derived using the method of Silvestro et al. (2020). For flux comparison purposes, all three bedform classes were characterized in the northeast ~1-2 km (upwind) section of the dune field based on image pair constraints (See SM section 2 for more details).

4.0 Results

4.1 Survey of polar megaripple occurrence

We surveyed dune fields imaged by HiRISE across all latitudes above 65°N to assess the presence or absence of intermediate-scaled bedforms (**Fig. 1**, **2a**). TARs and megaripples were classified separately based on their different size, albedo, and stratigraphic relationship (**Fig. 1**). TAR candidates were designated for light-toned, transverse bedforms, which were interpreted as being stratigraphically below dark dunes and meter-scale ripples (**Fig. 1b**). In contrast, megaripples were noted to be present for typically smaller, variable-

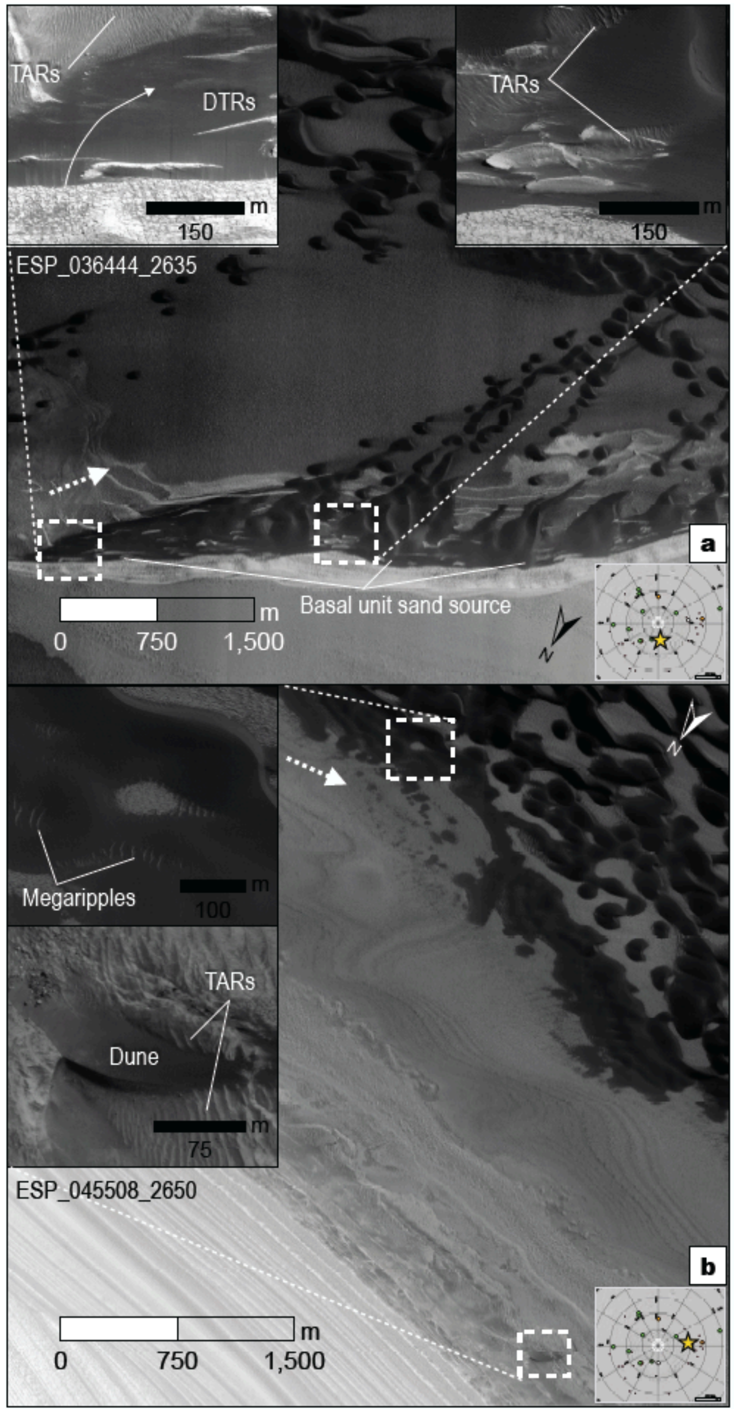

Figure 3. Examples of polar megaripples and TARs near the NPLD and basal unit sand sources at (a) Chasma Boreale and (b) west Olympia Cavi. Along with being underneath some dark dunes or ripples, polar TARs can be found superposed with boulders or with crests in opposing directions as nearby dunes transport. Approximate transport directions (dashed arrows) are shown. Inset maps show site locations (star).

albedo bedforms which were in most cases stratigraphically above or in continuity with neighboring bedforms (**Fig. 1a**). Of the 67 locations surveyed, 88.1% had megaripples, 9.0% had TARs, 9.0% had both, and 11.9% had neither class of intermediate-sized bedforms (**Table S2**). DTRs were found at all erg locations. Megaripples were commonly found upwind of erg areas, climbing dune slopes, or in small inter-dune fields. Bright-toned TARs were identified in large fields below scarps or under swifter dark bedforms, but dominantly nearest the NPLD-erg margins (**Fig. 2a, 3**, **4**). Likewise, the greatest proportion of HiRISE images lacking either intermediate-sized class were in these higher latitude areas (**Fig. 2a**, **S1**). Prior global surveys had described in passing the lack of TARs in polar regions compared with lower-latitude regions (Wilson and Zimbelman, 2004; Balme et al., 2008). More recently, Chojnacki et al. (2021) did a global HiRISE survey and identified close to half of all sites (52.5%) had bedforms identified as TARs (**Fig. 4**; **Table S2**).

4.2 Assessment of polar megaripple activity

To qualitatively and quantitatively assess the activity of polar megaripples we examined HiRISE long-baseline orthoimages (**Table S1**). Of the 13 monitoring sites in the north polar ergs, 85% (11) showed unambiguous migration of megaripples in (downwind) directions that are broadly aligned with that of nearby DTRs and dunes (**Fig. 2b**; **Animation S1-S5**). The remaining

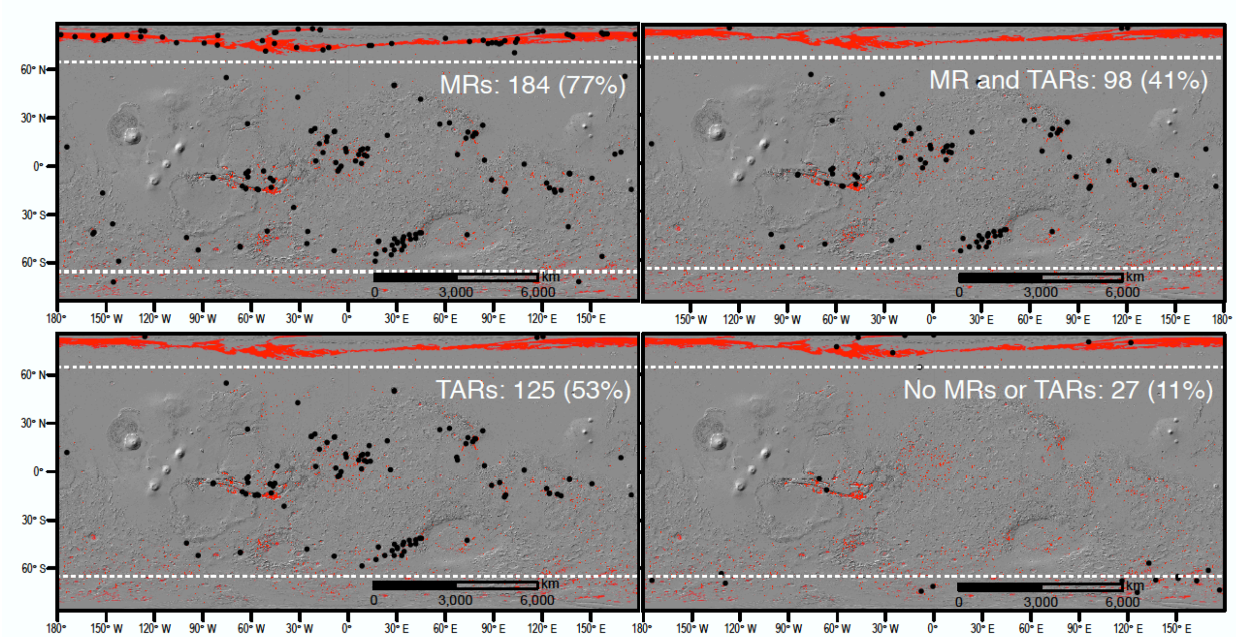

Figure 4. Global trends of intermediate-sized aeolian bedforms (black circles) using HiRISE images of dune fields. Megaripples (MR) and Transverse Aeolian Ridges (TARs) were classified separately based on their different size, albedo, and stratigraphic relationship. Compare with earlier MOC-based results (Wilson & Zimbelman, 2004). Base maps are MOLA shaded relief with dunes field in red (Hayward et al., 2014; Fenton, 2020).

Table 1. Polar megaripple activity results (Objective 2). Reported values are median ± median absolute deviations. The first two sites of McLaughlin crater and Nili Fossae are the lower latitude fields discussed by Silvestro, et al. (2020). Also see Fig. 2, 5.

Site ID and Name[a]	Elapsed time (EY)[b]	Displacement (m)	Migration rate (m/yr)	Wavelength (m)	Half average height (m)	Flux (m^3 m^{-1} yr^{-1})	N
3374+216 McLaughlin	7.57	0.97 ± 0.5	0.13 ± 0.06	6.7 ± 1	0.34 ± 0.05	0.042 ± 0.02	3215
0742+214 NiliFossae	9.38	1.4 ± 0.8	0.15 ± 0.09	7.1 ± 1	0.35 ± 0.05	0.051 ± 0.03	1828
2329+840 BuzzelDunes [c]	9.50	0.96 ± 0.4	0.1 ± 0.05	6.9 ± 0.9	0.34 ± 0.05	0.034 ± 0.02	2671
0953+761 PalmaDunes	9.33	1.4 ± 0.5	0.15 ± 0.06	7.8 ± 1	0.39 ± 0.05	0.056 ± 0.03	443
2121+790 GypsumErg	7.59	1 ± 0.2	0.13 ± 0.03	7.8 ± 0.6	0.39 ± 0.03	0.053 ± 0.01	302
1788+816 OlympiaUndae	7.47	1.1 ± 0.3	0.15 ± 0.04	8.7 ± 0.4	0.44 ± 0.02	0.064 ± 0.02	195
1035+703 LouthCrater	12.92	2.4 ± 0.4	0.19 ± 0.03	8.3 ± 1	0.42 ± 0.06	0.071 ± 0.02	200
1186+835 TleilaxDunes	11.00	1.8 ± 0.3	0.16 ± 0.03	8.8 ± 0.9	0.44 ± 0.05	0.069 ± 0.01	260
2798+809 AbalosScopuli	9.47	2.5 ± 0.6	0.26 ± 0.06	7.6 ± 1	0.38 ± 0.05	0.099 ± 0.03	375
2705+761 AbalosDunes	11.30	1.8 ± 0.3	0.16 ± 0.03	7.1 ± 1	0.36 ± 0.05	0.058 ± 0.01	370
3393+850 ChasmaBoreale	11.23	1.1 ± 0.4	0.095 ± 0.03	7.3 ± 1	0.36 ± 0.06	0.034 ± 0.01	521
2095+780 ScandiaCavi	11.27	1.2 ± 0.3	0.1 ± 0.02	9 ± 0.5	0.45 ± 0.02	0.045 ± 0.009	254
3154+827 ChasmaBoreale-MegadunesI	7.63	1.8 ± 0.6	0.24 ± 0.08	6.8 ± 0.9	0.34 ± 0.04	0.083 ± 0.03	145
All areas		1.2 ± 0.6	0.13 ± 0.06	7.1 ± 1	0.36 ± 0.06	0.046 ± 0.02	10779

[a]Dune field site IDs, where the first four digits are the monitoring site's centroid east longitude, the last three digits are the site's latitude (no decimals), and the "+" indicates the northern hemisphere. Informal site names are also provided where some correspond with those investigated by Diniega et al. (2017).

[b]See Table S1 for relevant HiRISE data information.

[c]The values for the Buzzel dunes correspond to the mapping of the full area (a total of 247 slip faces), while the measurements discussed in section 4.3 correspond to a buffer area (148 slip faces) shown in Fig. 6-7.

two sites had no megaripples present to observe, although DTRs and dunes were migrating at those locations (**Fig. S1**). Megaripple activity is most evident on the upwind edges of dune fields and in some cases within inter-erg areas or below arcuate scarps. Clusters of contiguous megaripple fields often flanked by ripples and dunes were most common, while occasionally occurrences of mobile megaripple trains atop of bedrock were observed (**Fig. 1a**, **Animation S3**). Crestlines may bifurcate, split, or merge with other megaripples moving at slower rates resulting in changes in crest-line patterns. In many cases, unambiguous megaripple migration was observed in shorter-term annual pairs as well (2-3 Mars years). Some of these swifter examples migrating several wavelengths made them difficult to track in longer baseline image pairs, whereas certain slower

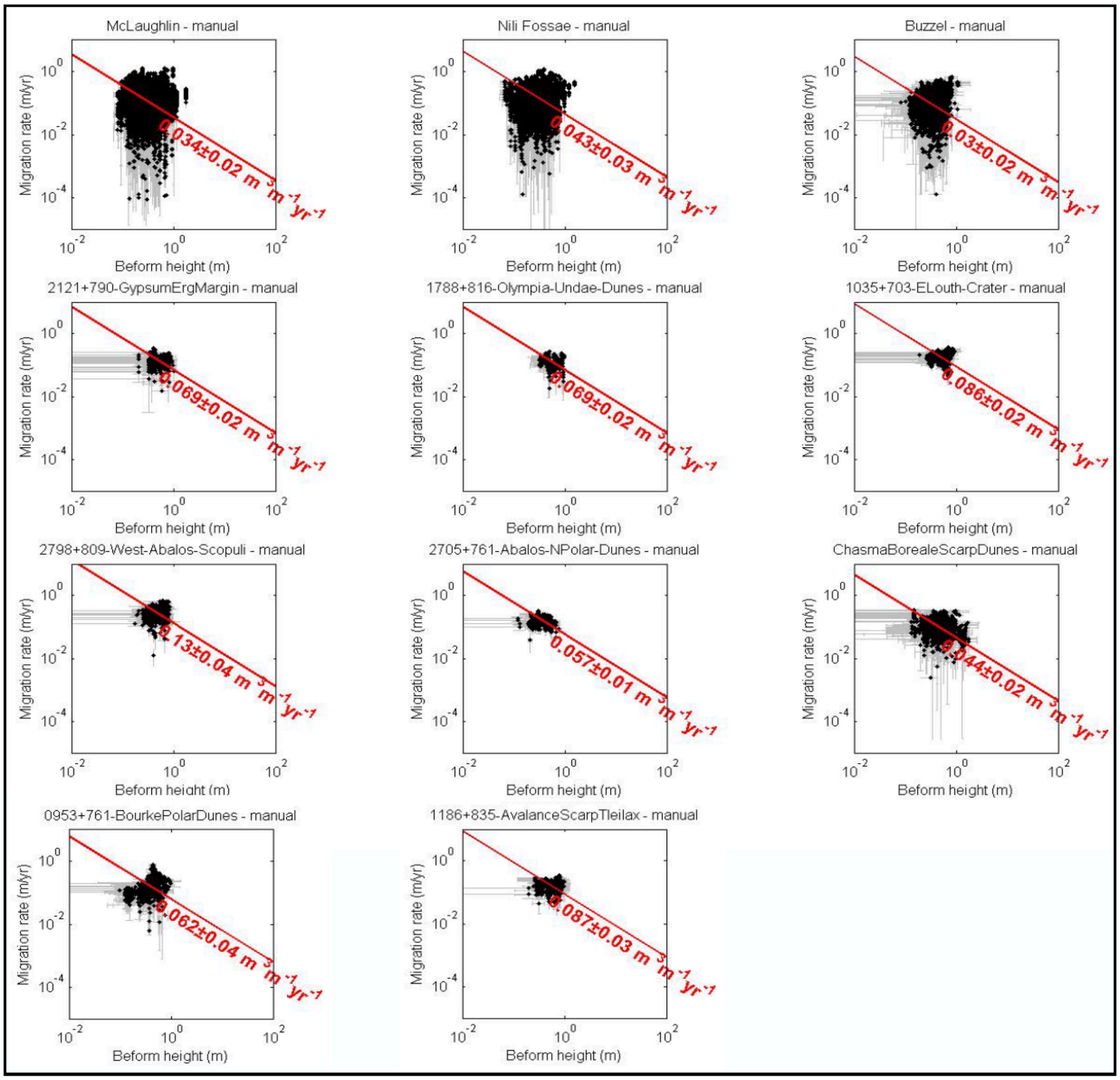

Figure 5. Megaripple sand flux results for 11 polar sites as compared with those in McLaughlin/Nili Fossae (top left two plots, Silvestro et al. 2020). Migration rates (y-axis) were derived from crestline mapping whereas heights (x-axis) were computed from wavelength-height relationships. Median sand fluxes (± median absolute deviation) are reported in red. Corresponding wavelength are provided in Fig. S2.

ones were overtaken and buried by dunes (**Animation S6-S7**). In contrast, all occurrences of polar TARs remained static at the time-scale and spatial resolution of this survey.

The median wavelength for active megaripple sites ranged between 5.8-11 m (average 7.2±2 m (**Fig. S2**); all reported uncertainties correspond to 1σ) and rates between 0.08-0.27 m/yr (0.13±0.06 m/yr for all sites)(**Fig. 5**; **Table 1; S2**). For comparison global average dune rates were ~0.5 m/yr (Chojnacki et al., 2019), average southern latitude ripple rates were 0.35 m/yr (Banks et al., 2018), and tropical latitude megaripples migrated at 0.12–0.13 m/yr (Silvestro et al., 2020). Average wavelength-derived heights for all sites were between 0.7-0.9 m (**Table 1**), but topographic profiles show some individual megaripples 1-2-m-tall (**Fig. S3**). The manually derived median megaripple sand fluxes ranged between 0.034-0.099 $m^3m^{-1}yr^{-1}$ (average q=0.046 ± 0.02 $m^3m^{-1}yr^{-1}$) (**Fig. 2b**, **5**; **Table 1**). Average sand dune crest fluxes for all but one of these sites (Louth crater) were moderate to high (7.4-18.6 $m^3m^{-1}yr^{-1}$) based on earlier measurements (**Fig. 2c;** (Chojnacki et al., 2019)). A comparison between the megaripple and sand dune flux distributions (**Fig. 2b-c**) shows a moderate correlation for monitoring sites implying a relation. That is, moderate to high flux dune fields tend to host a similar or lower megaripple flux classification, albeit threshold levels between flux classes are somewhat arbitrary. However, a more holistic approach is required to better understand the spatial and temporal aspects of megaripples within a given aeolian system (see **4.3**). Overall, we found that polar megaripple activity is widespread in various contexts (e.g., reentrant troughs, inter-ergs, polar craters), whereas static TAR candidates displayed rounded, broad, or pitted crests were found within otherwise active sand corridors adjacent to the NPLD (**Fig. 2b-2c**, **Animation S8**; see Section 5.2).

4.3 Polar megaripple fluxes and comparisons to other bedforms

The Buzzel site represents a typical polar trough dune field, which is located just downwind of its basal unit sand source (**Fig. 6**) (Fishbaugh and Head, 2005; Nerozzi and Holt, 2019). Proto dunes and sand sheets lead southwestward to more developed barchans and barchanoids as sediment supply increases (Ewing et al., 2015). In order to best constrain whole dune field fluxes we used a buffer area located on the upwind edge of the site (**Fig. 6a**), this way we obtained collocated flux measurements of all bedform classes. Sand dune migration rates (0.2-5.4 m/yr) and fluxes (1.1-35.7 $m^3m^{-1}yr^{-1}$) broadly decrease downwind to the southwest, but are quite variable in the cross-field directions (NW-SE)(**Fig. 7a, S4**; **Table 2**). Dune measurements were collected for two consecutive time periods (spanning 3.8 and 5.7 EY), resulting in similar fluxes, respectively 10.5±8 and 7.3±6 $m^3m^{-1}yr^{-1}$ average fluxes (**Fig. 6c, S4**, **Animation S9**).

Dark-toned ripples migrated at high rates throughout the site but are greatest along higher dune slopes and crests (**Fig. 7c**). Indeed, DTR migration rates ranged from 1-84 m/yr and averaged a high value of 9.6±6 m/yr in the brief period between images (L_s 94.96-105.08° or 22.6 days in MY35/2019). A longer baseline pair (L_s 105.08-128.4°) was investigated, but ripples had displaced too much for the COSI-Corr correlator to track them preventing a more precise computation of the migration rates. Associated DTRs fluxes were 0.2-10 $m^3m^{-1}yr^{-1}$ (average q=1.2 ± 0.8 $m^3m^{-1}yr^{-1}$) (**Fig. 7e**).

Megaripples are distributed across the study area but more often in the upwind locations (**Fig. 7b**). Megaripple sand fluxes here were 0.05-0.5 $m^3m^{-1}yr^{-1}$, which is similar to earlier analysis (see below). The very similar COSI-Corr (**Fig. 7b'**) and manually-derived (**Fig. 7b''**) megaripple rates (**Fig. 7e; Table 2**) illustrate the robustness of our

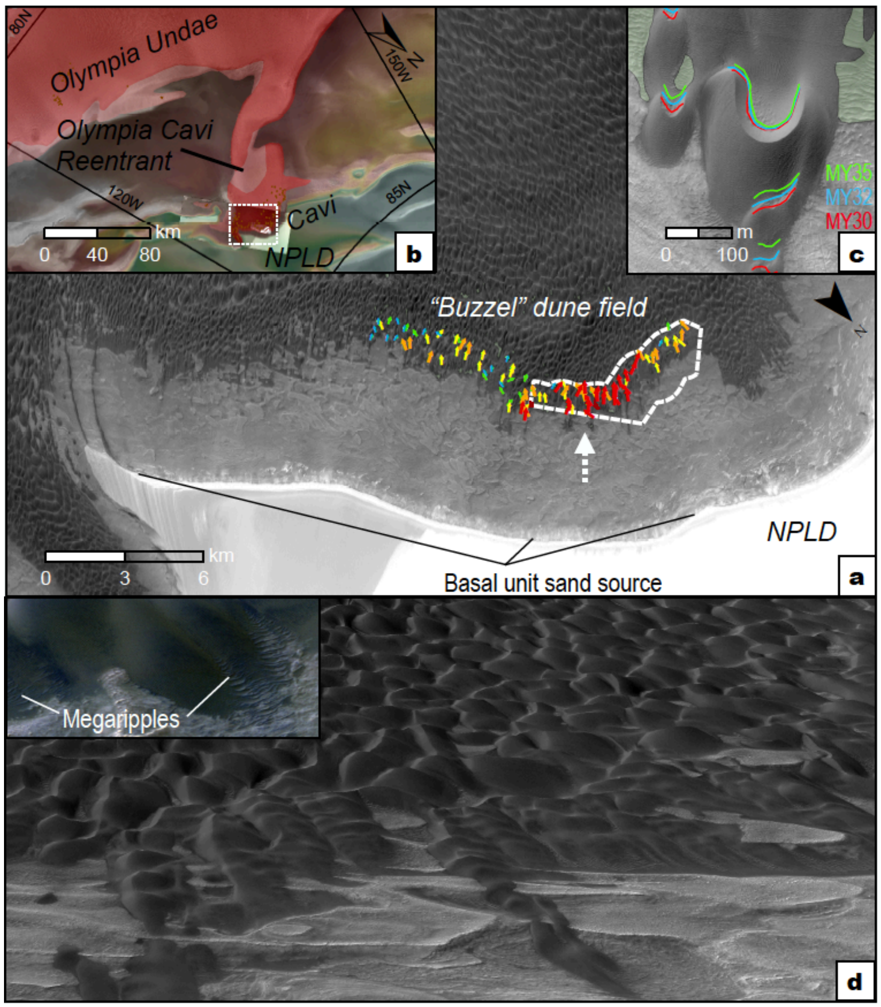

Figure 6. Context for the Buzzel study site. (a) View of the Buzzel site in Context Camera (CTX) images, where dune crest flux vectors (color arrows) are projected along with the buffer area (white polygon) for Objective 3's whole dune field flux analysis. Dunes are downwind of steep NPLD scarps and the regional sand source to the northeast. (b) Regional view showing the field-of-view for (a) (white box) with Buzzel at the head of the Olympia Cavi reentrant. CTX mosaic colorized with MOLA elevation. (c) Examples of dune lee face positions during 3 Mars years (MY) and nearby megaripples (green polygons). (d) Oblique view looking downwind (white arrow in (a)) from a projected orthoimage. (inset) Closer view of dunes and megaripples in HiRISE color.

analysis. Although megaripple crests that are armored by coarse grains are probably impervious

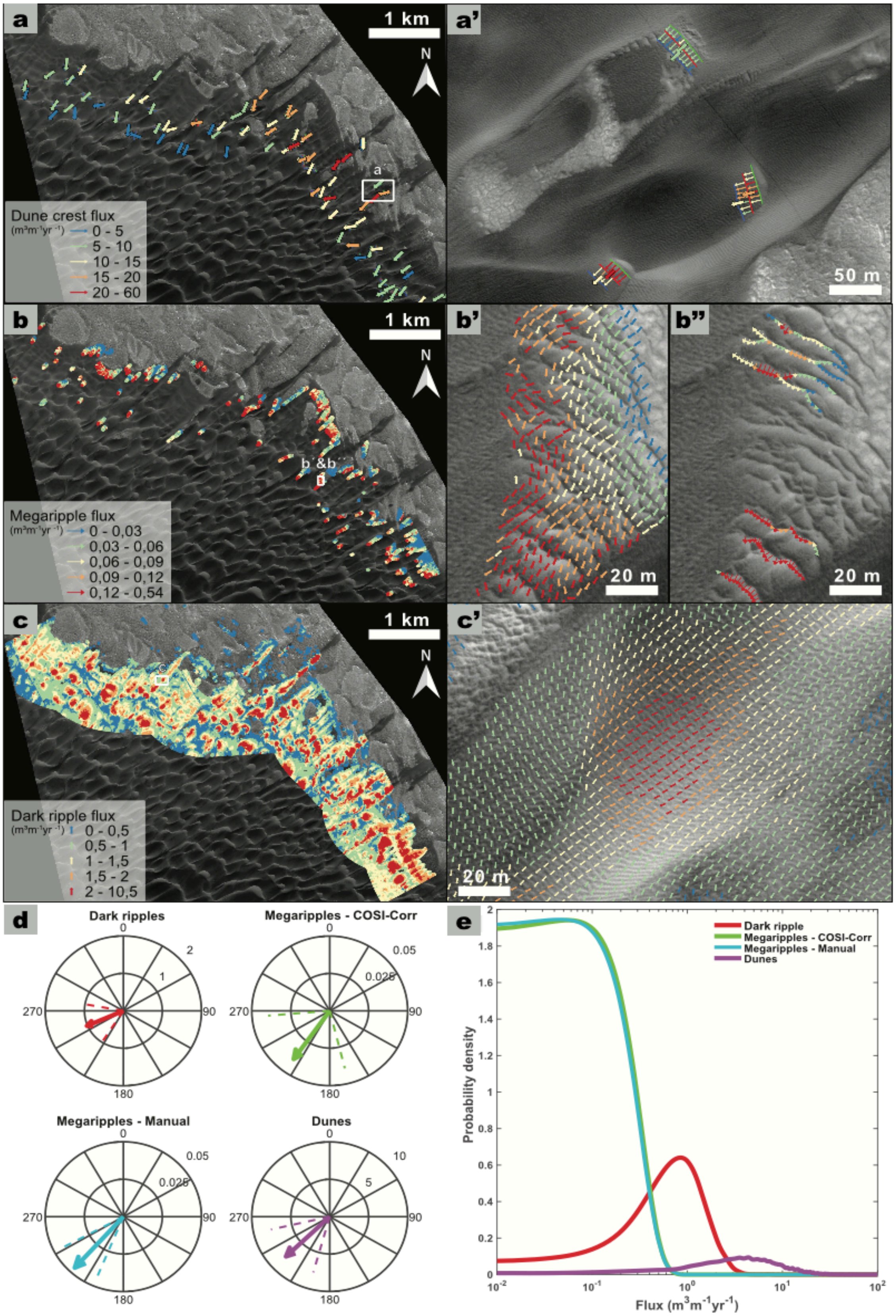

Figure 7. Comparison of the sand fluxes at the edge of the "Buzzel" dune field. Also see Fig. 6 for context, Fig. S4 for mapping examples, Fig. S5 for sand rose diagrams, Fig. S6 for COSI-Corr details, and Table 2 for summary statistics. (a) Sand dune crest flux results. (a´) Fluxes were evaluated at two time steps, spaced in time 3.8 and 5.7 EY. (b) Megaripple fluxes, which were estimated using two approaches: (b') automatic tracking of the bedforms with COSI-Corr, using a mask to select the intermediate scale bedforms and a constant half-height of 38 cm (corresponding to the average half-height estimated from the manual approach); and (b´´) manual mapping of bedform crest traces, which allowed migration rates and wavelength-derived bedform half-heights to be estimated (time interval of 9.5 EY). (c, c') Sand fluxes of meter-scale dark ripples that were quantified using COSI-Corr (for DTR displacements) and a constant half-height of 12.5 cm is assumed (time interval of 22.6 days). (d) Circular plots showing the fluxes mean vectors (m^3 $m^{-1}yr^{-1}$) and circular standard deviation intervals (dashed lines) for the bedforms and measurement techniques (in the case of the megaripples). (e) Flux comparisons for the Buzzel site bedforms that highlight the different modes of fluxes (fluxes distributions on the right), with megaripple's fluxes one and two orders of magnitude lower than DTR and dune crest fluxes, respectively.

to direct aeolian mobilization, copious amounts of DTR saltation events are available for creep transport. Note, megaripple rates are always lower than DTRs or dunes, indicating they don't contribute to total crest fluxes since they never or infrequently approach dune brinks. Instead megaripple populations are overtaken and occasionally buried by swifter dunes or DTR groups (**Animation S6-S7**). Active megaripples migration trends (216±50°) are closely aligned with those of dunes (226±31°), whereas migrating DTRs (247±34°) show a more westward trend (**Fig. 7d**, **S5**). Overall, it is estimated that the advancement of megaripples, reptation of DTRs, and dune slip face avalanches account for ~1%, ~10%, and ~100%, respectively, of the sand fluxes at the Buzzel dune field (**Fig. 7e**).

It is worthwhile to compare these results with non-polar megaripple sites. For example, dune crest fluxes at tropical latitudes in Nili Fossae and McLaughlin are ~3 $m^3m^{-1}yr^{-1}$, while fluxes derived for the megaripples in the same regions are two orders of magnitude lower (0.03-0.04 $m^3m^{-1}yr^{-1}$) (Silvestro et al., 2020). Therefore, despite the higher magnitude of fluxes (more than double) and differing boundary conditions at the polar site, we observe a similar relation between the megaripples reptation and slip face advancement fluxes (~1%).

Dark-toned ripple reptation fluxes in Nili Patera were found to correspond to 20% of the slip face fluxes (6.9 $m^3m^{-1}yr^{-1}$; Bridges et al., 2012). Slower ripples at the Herschel crater dune field were estimated to have lower reptation fluxes (0.06 $m^3m^{-1}yr^{-1}$, see SM; Cardinale et al., 2016), which would equate to ~5% of the bulk flux there (1.2 $m^3m^{-1}yr^{-1}$; Vaz et al., 2017). A similar relationship is found for the Bagnold dune field located in Gale crater, where a reptation/bulk flux partition of 4% is estimated (Silvestro et al., 2016, 2020). Overall, the mentioned DTRs reptation fluxes represent 4-20% of the bulk sedimentary flux inferred from the slip face advancements, in

Table 2. Summary statistics for the compared bedforms' fluxes. The reported values correspond to a common area, located up to 1 km from the dune field edge at the Buzzel site (**Fig. 7**, **6**).

	Mean flux azimuth (˚)	Mean flux magnitude ($m^3\ m^{-1}yr^{-1}$)	Circular variance	Circular STD (˚)	N	Average flux ($m^3\ m^{-1}yr^{-1}$)	Flux STD ($m^3\ m^{-1}yr^{-1}$)
Dark-toned ripples	246.7	1.01	0.16	33.5	373172	1.2	0.77
Megaripples - COSI-Corr	215.6	0.04	0.31	49.8	27562	0.06	0.05
Megaripples - Manual	222.3	0.05	0.06	19.7	2758	0.05	0.05
Dune crest flux	226.4	7.73	0.13	30.7	9706	8.92	7.4

line with the 10% estimate for the Buzzel polar site. In addition, there appears to be a positive correlation between bulk crest fluxes and the relative weight of DTR reptation fluxes, which will be tested in the future.

5.0 Discussion

5.1 Spatial heterogeneity of polar intermediate-scale bedforms

North polar megaripples and TARs show spatial heterogeneity in their distribution motivating the question – *why are these bedforms relatively abundant at some north polar sites, but absent at others?* Survey results indicate aeolian megaripples are widespread in the north polar region particularly for areas of higher dune density or sand volume (**Fig. 2a**, **4**). If the identified bedforms are truly composed of bimodal sand this indicates an abundant coarse-grained sand population is present for the ergs – an interesting revelation considering the regional sand source. The consensus view holds most regional sand is sourced from basal cavi units underlying the NPLD (**Fig. S1**) (Byrne and Murray, 2002; Fishbaugh and Head, 2005; Tanaka et al., 2008). Based on cross-bedding exposures, internal radar reflections, compositional links, and propensity to produce sand the cavi units are widely agreed to be elements of a massive buried erg by an expanding ice cap (Massé et al., 2010; Brothers et al., 2018; Nerozzi and Holt, 2019). The presence of an ample coarse sand population, as inferred for megaripples based on their greater size and bright crests, suggests the paleo-erg source was not mature enough to be dominated by fine, well sorted sand. That is, a recycled sand source that has gone through repeated periods of sedimentation (i.e., aeolian sandstone units) (Edgett et al., 2020) is more likely to be rich in fine sand, as compared with a primary sand source (i.e., volcaniclastic units)(Kocurek and Lancaster, 1999; Chojnacki et al., 2014).

In contrast, there are certain sand transport corridors which lack both megaripples or TARs. For example, the low sand density barchans and ripples of the west Olympia Cavi reentrant (**Fig. 2a;** 110°E, 81°N) are largely without intermediate-bedforms. Other inter-erg areas mapped with low to moderate sand coverage by Hayward et al. (2014) are similar (**Fig. 2a**). In these locations, scattered barchans or dome dunes migrate in low sediment supply conditions (**Fig. S1**), and are apparently deficient in a coarse sand population conducive to megaripple formation. These aeolian systems maybe ultimately sourced by a more mature (finer-grained) sand supply or have migrated far downwind of any accompanying coarser-sand megaripple population.

Interestingly, bedforms with characteristics commonly attributed to TARs (e.g. light-toned, transverse, >20 m in spacing) are generally absent in most polar regions except at the higher latitude NPLD-erg contact areas (**Fig. 2a**, **4**, **8**). The north polar TAR candidates identified generally appeared weathered, cracked, with rounded or "boxy" crests, or partially buried (as do some lower latitude examples (Sullivan et al., 2008; Chojnacki et al., 2018)), consistent with long-term inactivity (**Fig. 1a**, **8**). Indeed, a detailed study in Scandi Cavi by Fenton et al. (2021) estimated a lower limit age of TAR-like bedforms there to be ~270 kyrs. Additionally, we suggest the stability and appearance for some polar TARs is most readily explained by an inter-granular ice component (see Section 5.2). Their close proximity to scarps (the likely regional sand source) and lack of mobility may suggest regional polar TARs did not migrate far after formation.

5.2 Sand fluxes of polar megaripples and the seasonal cycle

Prior work has suggested that north polar dune systems are more active than elsewhere – ~50% greater sand dune crest fluxes than on average for Mars (11.4 vs. 7.8 m^3 m^{-1} yr^{-1}) (Chojnacki et al., 2019). The high magnitude of migration and flux rates of Buzzel's DTRs, megaripples, and dunes (**Fig. 7**) would support this notion. It is noted, the cross-bedform comparison for Buzzel required the upwind (**Fig. 6**) and arguably most dynamic sections of the dune field to be analyzed – this was unavoidable due to data coverage. Nevertheless, this high level of bedform activity is somewhat surprising due to the short period (northern summer and autumn) for frost-free sediment availability (Hansen et al., 2013, 2015; Chojnacki et al., 2019). An important relevant question pertains to whether polar seasonal processes promote or retard megaripple activity. At a broadscale the unique surface-atmospheric volatile interactions found at the martian north pole and resulting wind regime is likely a governing factor for the observed enhanced megaripple migration. The north polar wind regime is dominated by off-cap katabatic 'sublimation winds', which are modeled to be greatest in magnitude, consistent in direction, and perhaps more persistent throughout the polar day during the late spring-summer than elsewhere on Mars (Massé et al., 2012; Smith and Spiga, 2018). Winds are driven by seasonal and thermal effects of the retreating spring/summer CO_2 ice and strong contrast between polar cap and erg surfaces in terms of elevation (~2 km-high), temperature (23 K), and albedo (15-25%) (Howard, 2000; Smith and Spiga, 2018; Chojnacki et al., 2019). These seasonally forced winds and occasional storm events (Wang and Fisher, 2009;

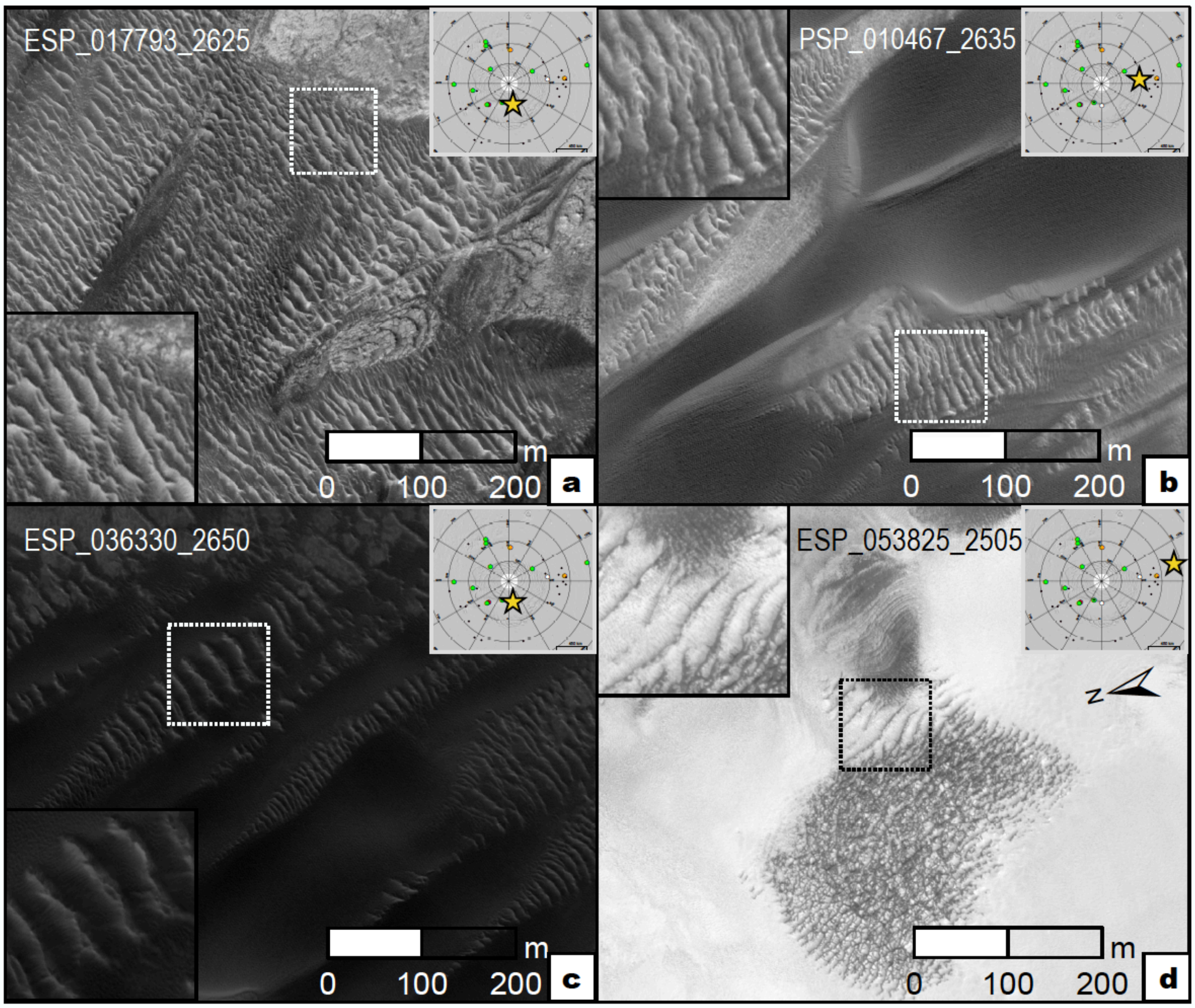

Figure 8. Polar erg sites with progressively more degraded TARs or megaripples (top left and working clockwise). All sites are for inactive bedforms that appeared weathered, cracked, with rounded or "boxy" crests, or partially buried. These static bedforms often show nearby mobile megaripples and DTRs without similar morphologic characteristics. (a) Chasma Boreale, (b) west Olympia Cavi, (c) Chasma Boreale, and (d) Louth crater. Inset maps show site locations (star) and HiRISE insets are 100-m-wide.

Calvin et al., 2015) appear to drive the high frequency megaripple activity in the region (**Fig. 2**, **7**).

What about more direct evidence of polar processes impacting bedform movement at a finer scale? For example, following summertime oversteepening by aeolian processes (Horgan and Bell, 2012) dune slip face alcove formation is seasonally constrained to the autumn/winter, further expanded during springtime frost sublimation, and estimated to contribute to 2-20% of dune movement (Hansen et al., 2015; Diniega et al., 2017). A similar process of seasonal fracturing and wasting of steeper megaripple lee-ward faces may lead to movement, even under frost veneers (**Fig. 9**). However, it is unclear that bulk megaripple displacements and their direction(s), which is well-correlated with that of the nearby bedforms (**Fig. 7d**), are dominantly caused by cryosphere processes. Most megaripple lee and stoss areas appear to be relatively symmetric and not substantially steeper on the lee-side, which might cause oversteepening and mini-alcoves. Although these features would be challenging to track, lee-side slumps or alcoves on megaripples are not clearly evident even when fully illuminated. Additionally, Buzzel's relative flux partitions between bedform classes are comparable to other equatorial dune fields, suggesting that primary aeolian transport modes (impact-driven creep and reptation + saltation) are driving most of the activity in the polar sites, instead of ice-related seasonal processes.

Instead, the cyclical deposition of CO_2/H_2O frost and ice has an important role in regional bedform stabilization over different time frames (Schatz et al., 2006; Brothers et al., 2018). Dark material with icy foresets, isolated dunes, cross-bedded strata and bounding surfaces have been identified in either cavi scarp units or interdune areas, which are interpreted as various components of an ancient aeolian sand sea related to past climate change (Ewing et al., 2010; Brothers et al., 2018; Nerozzi and Holt, 2019). Certain modern duneforms also show evidence for cross-stratified ice, partial burial by residual frost (**Fig. 1e**, **8**), and thermal properties consistent with a shallow ice table (<1 m and as low as ~3 cm deep) (Putzig et al., 2014; Brothers and Kocurek, 2018). We suggest these cryospheric processes impact intermediate-scale bedforms as well and help explain the degraded morphology of some TAR-like bedforms. Polar TARs that are often characterized by weathered, occasionally pitted, or rounded crests that remain static despite being located in active sand pathways (**Fig. 1b**, **8**; **Animation S8**). More extreme examples can be found of TARs buried in late season frost or perennial water ice (**Fig. 1c**, **8b**). In these cases, volatile-related processes and any accompanying cohesion may have outpaced bedform mobility. An analogous process has been described for lower-latitude immobile bedforms which display evidence for dry-condition induration (e.g., cohesion, chemical weathering) and are thought to occur over long periods of inactivity (Sullivan et al., 2008, 2020).

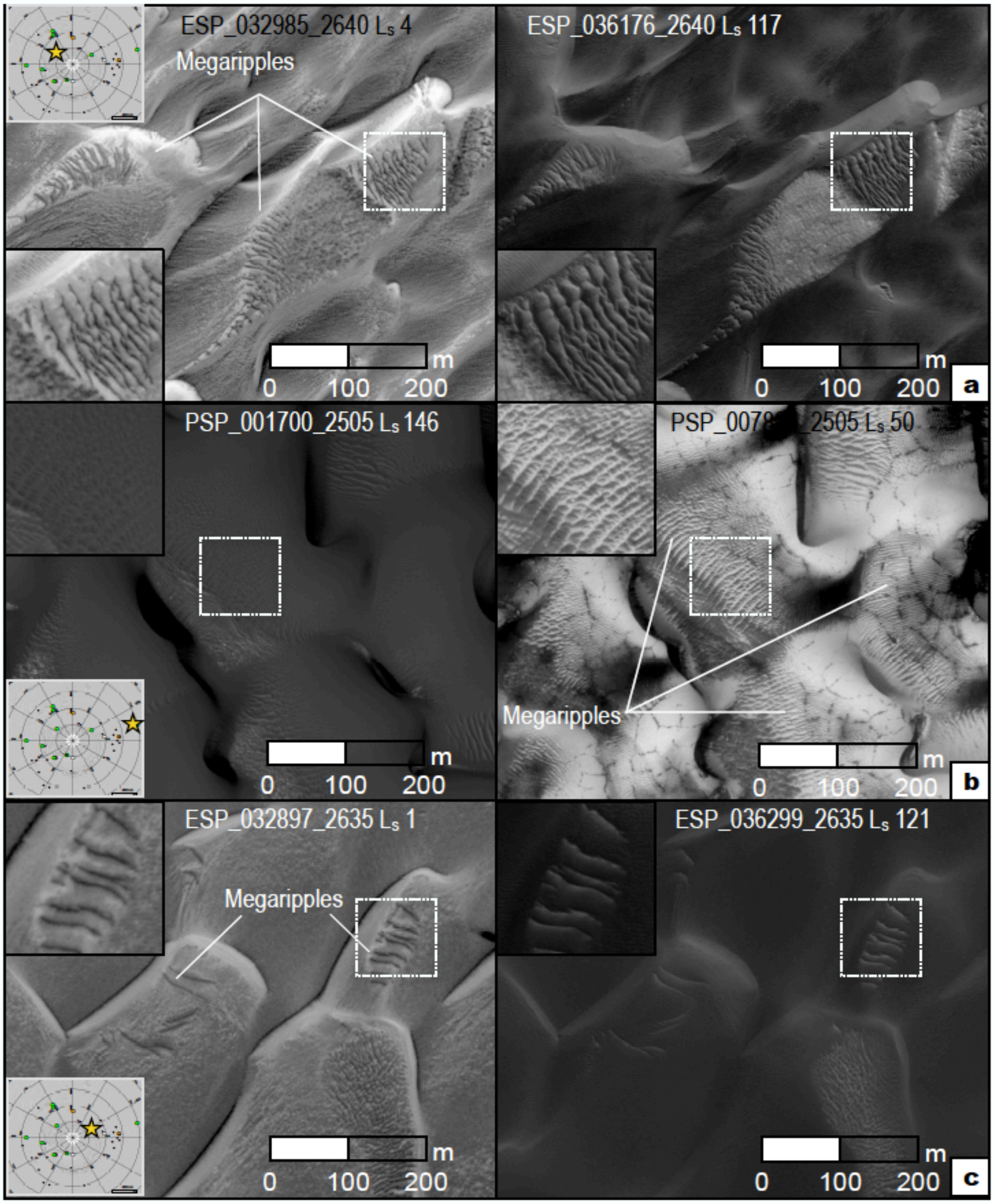

Figure 9. Seasonal changes between northern spring and summer for polar megaripples and dunes. All sites are for active megaripples. (a) Buzzel dunes in east Olympia Cavi reentrant, (b) Loath crater, and (c) West Olympia Cavi reentrant. Inset maps show site locations (star) and HiRISE insets are 100-m-wide.

In contrast to the static possibly ice-cemented polar TARs, megaripples in the same environment remain mobile over many polar winters even when temporarily buried then exhumed by swifter duneforms (**Animation S6-S7**). Whereas spring ice does not fill in megaripple troughs (estimated to be ~1 meter; e.g., **Fig. S3**), DTR areas appear to be smoothed over, suggesting decimeter-thick winter frost accumulation (**Fig. 9**). CO_2 frost is typically fully sublimated off sandy surfaces by late spring (L_s ~80-90°) (Hansen et al., 2013; Portyankina et al., 2013), possibly slightly earlier for sites like Buzzel where slip faces are orientated southward (Pommerol et al., 2013). DTRs and megaripple surfaces are able to respond to wind and regain mobility promptly around the northern summer solstice. While many of the boundary conditions are nearly identical for the adjacent populations of polar megaripples and TARs (e.g., seasonal cycle, wind regime, topography), sand availability for saltation/creep and inter-grain ice-content may be large factors in determining mobile vs. immobile.

6.0 CONCLUSIONS

This effort identified the presence, activity, and sand flux contribution of intermediate-scale aeolian bedforms across the north polar erg. The megaripple populations found at these locations were found to be migrating with dunes and dark-toned ripples when adequate data was inspected. Other key findings include the following:

- While megaripples are relatively minor components of terrestrial aeolian systems they are abundant on Mars and the north polar erg. Bedforms identified as TARs display characteristics consistent with inactivity (e.g., rounded or pitted crests) and are primary concentrated at the base of the polar layered deposit scarps and nearby erg areas. These (static) bedforms are adjacent to the regional sand source of the basal unit, which suggests polar TARs do not migrate far after formation.
- A lesser amount of polar aeolian systems, often on erg margins, lack megaripples but show widespread and mobile ripples and dunes (e.g., west Olympia Cavi reentrant). These areas are under low sediment supply conditions where widely-separated low sand volume barchan/dome dunes migrate. These areas may lack a particle size distribution conducive to megaripple formation (i.e., no coarse sand size fraction).
- Megaripples are highly active in the north polar region including NPLD reentrants (e.g., Chasma Boreale), interior-erg areas, and polar craters (**Fig. 2**). The high level of observed activity seems to be associated with high sand fluxes of dunes, despite the

limited sediment availability when sandy areas are under autumn, winter, and spring CO_2 frost and ice (Hansen et al., 2013; Chojnacki et al., 2019).

- A focused analysis of an Olympia Cavi reentrant aeolian system estimated that the advancement of megaripples, saltation and reptation of DTRs, and dune slip face avalanches account for ~1%, ~10%, and ~100%, respectively, of the sand fluxes (**Fig. 7**). To our knowledge DTR and dune rates are some of the highest yet documented on Mars, yet the flux partition between the various bedforms does not seem to differ from equatorial sites with lower sand fluxes.
- Polar megaripples yield fluxes that are two orders of magnitude lower than neighboring dunes, consistent with earlier work (Silvestro et al., 2020). While these bedforms do not show significantly greater migration rates or fluxes, activity does occur with a higher frequency across the polar ergs than lower latitudes, possibly due to the greater occurrence of high seasonal winds.
- Whereas seasonal ice contributes to some bedforms movement, such as dune slip face alcoves (Diniega et al., 2017), no evidence was found that cryospheric processes directly promoted megaripple migration. However, late spring-summer off-cap katabatic 'sublimation winds' along with polar storm induced winds are deemed major factors for the high levels of observed bedform activity.

ACKNOWLEDGMENTS: For M.C. & S.S. this research was supported in part by NASA Mars Data Analysis Program Grant 80NSSC20K1066 and the HiRISE/MRO mission. D.A.V. & D.C.A.S. acknowledge CITEUC's support (UID/Multi/00611/2021&POCI-01-0145-FEDER-006922), FCT (Grant CEECIND/02981/2017), and the Laboratory for Advanced Computing at University of Coimbra for providing computing resources. We would like to thank HiRISE operations staff with assistance in targeting and UArizona student Kris Akers for DTM production. Helpful conversations with Ryan Ewing and James Zimbelman are greatly appreciated. Supporting information is available in the online version of the paper, including supplemental methodology, tables, figures, and data tables (for Fig. S1-S6). All of the data used for this investigation can be found at the HiRISE website (http://hirise.lpl.arizona.edu/) or the Planetary Data System (https://pds-geosciences.wustl.edu/missions/mep/index.htm).

REFERENCES CITED:

Bagnold, R.A., 1941, The Physics of Blown Sand and Desert Dunes: London, Methuen, 265 p.

Balme, M., Berman, D.C., Bourke, M.C., and Zimbelman, J.R., 2008, Transverse Aeolian Ridges (TARs) on Mars: Geomorphology, v. 101, p. 703–720, doi:10.1016/j.geomorph.2008.03.011.

Banks, M.E., Fenton, L.K., Bridges, N.T., Geissler, P.E., Chojnacki, M., Runyon, K.D., Silvestro, S., and Zimbelman, J.R., 2018, Patterns in Mobility and Modification of Middle- and High-Latitude Southern Hemisphere Dunes on Mars: Journal of Geophysical Research: Planets, doi:10.1029/2018JE005747.

Berman, D.C., Balme, M.R., Michalski, J.R., Clark, S.C., and Joseph, E.C.S., 2018, High-resolution investigations of Transverse Aeolian Ridges on Mars: Icarus, v. 312, p. 247–266, doi:10.1016/j.icarus.2018.05.003.

Bourke, M., Edgett, K., and Cantor, B., 2008, Recent aeolian dune change on Mars: Geomorphology, v. 94, p. 247–255, doi:10.1016/j.geomorph.2007.05.012.

Bridges, N.T. et al., 2011, Planet-wide sand motion on Mars: Geology, v. 40, p. 31–34, doi:10.1130/G32373.1.

Bridges, N.T., Ayoub, F., Avouac, J.-P., Leprince, S., Lucas, A., and Mattson, S., 2012, Earth-like sand fluxes on Mars: Nature, v. 485, p. 339–342, doi:10.1038/nature11022.

Brothers, S.C., and Kocurek, G., 2018, The transitional depositional environment and sequence stratigraphy of Chasma Boreale: Icarus, v. 308, p. 27–41, doi:10.1016/j.icarus.2017.08.038.

Brothers, S.C., Kocurek, G., and Holt, J.W., 2018, Sequence architecture of the cavi unit, Chasma Boreale, Mars: Icarus, v. 308, p. 42–60, doi:10.1016/j.icarus.2017.06.024.

Byrne, S., and Murray, B.C., 2002, North polar stratigraphy and the paleo-erg of Mars: Journal of Geophysical Research: Planets, v. 107, p. 11–1, doi:10.1029/2001JE001615.

Calvin, W.M., James, P.B., Cantor, B.A., and Dixon, E.M., 2015, Interannual and seasonal changes in the north polar ice deposits of Mars: Observations from MY 29–31 using MARCI: Icarus, v. 251, p. 181–190, doi:10.1016/j.icarus.2014.08.026.

Cardinale, M., Silvestro, S., Vaz, D.A., Michaels, T., Bourke, M.C., Komatsu, G., and Marinangeli, L., 2016, Present-day aeolian activity in Herschel Crater, Mars: Icarus, v. 265, p. 139–148, doi:10.1016/j.icarus.2015.10.022.

Chojnacki, M., Banks, M.E., Fenton, L.K., and Urso, A.C., 2019, Boundary condition controls on the high-sand-flux regions of Mars: Geology, doi:10.1130/G45793.1.

Chojnacki, M., Banks, M., and Urso, A., 2018, Wind-Driven Erosion and Exposure Potential at Mars 2020 Rover Candidate-Landing Sites: Journal of Geophysical Research: Planets, v. 123, p. 468–488, doi:10.1002/2017JE005460.

Chojnacki, M., Burr, D.M., Moersch, J.E., and Wray, J.J., 2014, Valles Marineris dune sediment provenance and pathways: Icarus, v. 232, p. 187–219, doi:10.1016/j.icarus.2014.01.011.

Chojnacki, M., Johnson, J.R., Moersch, J.E., Fenton, L.K., Michaels, T.I., and Bell III, J.F., 2015, Persistent aeolian activity at Endeavour crater, Meridiani Planum, Mars; new observations from orbit and the surface: Dynamic Mars, v. 251, p. 275–290, doi:10.1016/j.icarus.2014.04.044.

Diniega, S., Hansen, C.J., Allen, A., Grigsby, N., Li, Z., Perez, T., and Chojnacki, M., 2017, Dune-slope activity due to frost and wind throughout the north polar erg, Mars: Geol. Soc., London, v. 467, p. 95–114, doi:10.1144/SP467.6.

Edgett, K.S. et al., 2020, Extraformational sediment recycling on Mars: Geosphere, v. 16, p. 1508–1537, doi:10.1130/GES02244.1.

Ewing, R.C., McDonald, G.D., and Hayes, A.G., 2015, Multi-spatial analysis of aeolian dune-field patterns: Geomorphology, v. 240, p. 44–53, doi:10.1016/j.geomorph.2014.11.023.

Ewing, R.C., Peyret, A.-P.B., Kocurek, G.A., and Bourke, M., 2010, Dune field pattern formation and recent transporting winds in the Olympia Undae Dune Field, north polar region of Mars: Journal of Geophysical Research: Planets, v. 115, p. E08005, doi:10.1029/2009JE003526.

Fenton, L.K., 2020, Updating the global inventory of dune fields on Mars and identification of many small dune fields: Icarus, v. 352, p. 114018, doi:10.1016/j.icarus.2020.114018.

Fenton, L.K., Silvestro, S., and Kocurek, G., 2021, Transverse Aeolian Ridge Growth Mechanisms and Pattern Evolution in Scandia Cavi, Mars: Frontiers in Earth Science, v. 8, p. 619704, doi:10.3389/feart.2020.619704.

Fishbaugh, K.E., and Head, J.W., 2005, Origin and characteristics of the Mars north polar basal unit and implications for polar geologic history: Icarus, v. 174, p. 444–474, doi:10.1016/j.icarus.2004.06.021.

Geissler, P.E., and Wilgus, J.T., 2017, The morphology of transverse aeolian ridges on Mars: Aeolian Research, v. 26, p. 63–71, doi:10.1016/j.aeolia.2016.08.008.

Greeley, R., and Iversen, J.D., 1985, Wind as a geological process on Earth, Mars, Venus and Titan (R. Greeley, Ed.): New York, Cambridge Univ. Press, 332 p.

Greeley, R., Lancaster, N., Lee, S.W., and Thomas, P.C., 1992, Martian Aeolian Processes, Sediments and Features, *in* Kieffer, H.H., Jakosky, B.M., Snyder, C.W., and Matthews, M.S. eds., Mars, Tucson, University of Arizona Press, Space science series., p. 730–766.

Hansen, C.J. et al., 2011, Seasonal Erosion and Restoration of Mars' Northern Polar Dunes: Science, v. 331, p. 575–578, doi:10.1126/science.1197636.

Hansen, C.J., Byrne, S., Portyankina, G., Bourke, M., Dundas, C., McEwen, A., Mellon, M., Pommerol, A., and Thomas, N., 2013, Observations of the northern seasonal polar cap on Mars: I. Spring sublimation activity and processes: Mars Polar Science V, v. 225, p. 881–897, doi:10.1016/j.icarus.2012.09.024.

Hansen, C.J., Diniega, S., Bridges, N., Byrne, S., Dundas, C., McEwen, A., and Portyankina, G., 2015, Agents of change on Mars' northern dunes: CO2 ice and wind: Icarus, v. 251, p. 264–274, doi:10.1016/j.icarus.2014.11.015.

Hayward, R.K., 2011, Mars Global Digital Dune Database (MGD3): north polar region (MC-1) distribution, applications, and volume estimates: Earth Surface Processes and Landforms, v. 36, p. 1967–1972, doi:10.1002/esp.2219.

Hayward, R.K., Fenton, L.K., and Titus, T.N., 2014, Mars Global Digital Dune Database (MGD3): Global dune distribution and wind pattern observations: Icarus, v. 230, p. 38–46, doi:10.1016/j.icarus.2013.04.011.

Horgan, B.H.N., and Bell, J.F., 2012, Seasonally active slipface avalanches in the north polar sand sea of Mars: Evidence for a wind-related origin: Geophys. Res. Lett., v. 39, p. L09201, doi:10.1029/2012GL051329.

Howard, A., 2000, The Role of Eolian Processes in Forming Surface Features of the Martian Polar Layered Deposits: Icarus, v. 144, p. 267–288, doi:10.1006/icar.1999.6305.

Hugenholtz, C.H., and Barchyn, T.E., 2017, A terrestrial analog for transverse aeolian ridges (TARs): Environment, morphometry, and recent dynamics: Icarus, v. 289, p. 239–253, doi:10.1016/j.icarus.2016.08.010.

Isenberg, O., Yizhaq, H., Tsoar, H., Wenkart, R., Karnieli, A., Kok, J.F., and Katra, I., 2011a, Megaripple flattening due to strong winds: Geomorphology, v. 131, p. 69–84, doi:10.1016/j.geomorph.2011.04.028.

Isenberg, O., Yizhaq, H., Tsoar, H., Wenkart, R., Karnieli, A., Kok, J.F., and Katra, I., 2011b, Megaripple flattening due to strong winds: Geomorphology, v. 131, p. 69–84, doi:10.1016/j.geomorph.2011.04.028.

Khayat, A.S.J., Smith, M.D., and Guzewich, S.D., 2019, Understanding the water cycle above the north polar cap on Mars using MRO CRISM retrievals of water vapor: Icarus, v. 321, p. 722–735, doi:10.1016/j.icarus.2018.12.024.

Kirk, R.L. et al., 2008, Ultrahigh resolution topographic mapping of Mars with MRO HiRISE stereo images: Meter-scale slopes of candidate Phoenix landing sites: Journal of Geophysical Research, v. 113, doi:10.1029/2007JE003000.

Kocurek, G.A., and Ewing, R.C., 2012, Source-To-Sink: An Earth/Mars Comparison of Boundary Conditions for Aeolian Dune Systems., *in* Grotzinger, J.P., Grotzinger, J.P., and Milliken, R.E. eds., Sedimentary geology of Mars, Tulsa, Okla, SEPM (Society for Sedimentary Geology), SEPM special publication no. 102, p. 18.

Kocurek, G., and Lancaster, N., 1999, Aeolian system sediment state: theory and Mojave Desert Kelso dune field example: Sedimentology, v. 46, p. 505–515, doi:10.1046/j.1365-3091.1999.00227.x.

Lancaster, N., 2009, Dune Morphology and Dynamics, *in* Parsons, AnthonyJ. and Abrahams, AtholD. eds., Geomorphology of Desert Environments, Chapter 18, Springer Netherlands, p. 557–595, http://dx.doi.org/10.1007/978-1-4020-5719-9_18.

Langevin, Y., 2005, Summer Evolution of the North Polar Cap of Mars as Observed by OMEGA/Mars Express: Science, v. 307, p. 1581–1584, doi:10.1126/science.1109438.

Lapotre, M.G.A. et al., 2016, Large wind ripples on Mars: A record of atmospheric evolution: Science, v. 353, p. 55–58, doi:10.1126/science.aaf3206.

Lapotre, M.G.A., Ewing, R.C., Weitz, C.M., Lewis, K.W., Lamb, M.P., Ehlmann, B.L., and Rubin, D.M., 2018, Morphologic Diversity of Martian Ripples: Implications for Large-Ripple Formation: Geophysical Research Letters, doi:10.1029/2018GL079029.

Leprince, S., Barbot, S., Ayoub, F., and Avouac, J.P., 2007, Automatic, Precise, Ortho-rectification and Coregistration for satellite Image Correlation, Application to Ground Deformation Measurement: IEEE J. Geosci. Rem. Sens., v. 45, p. 1529–1558.

Lorenz, R.D., and Valdez, A., 2011, Variable wind ripple migration at Great Sand Dunes National Park and Preserve, observed by timelapse imaging: Geomorphology, v. 133, p. 1–10, doi:10.1016/j.geomorph.2011.06.003.

Malin, M.C., and Edgett, K.S., 2001, Mars Global Surveyor Mars Orbiter Camera: Interplanetary cruise through primary mission: Journal of Geophysical Research, v. 106, p. 23429–23570, doi:10.1029/2000JE001455.

Massé, M., Bourgeois, O., Le Mouélic, S., Verpoorter, C., Le Deit, L., and Bibring, J.P., 2010, Martian polar and circum-polar sulfate-bearing deposits: Sublimation tills derived from the North Polar Cap: Icarus, v. 209, p. 434–451, doi:10.1016/j.icarus.2010.04.017.

Massé, M., Bourgeois, O., Le Mouélic, S., Verpoorter, C., Spiga, A., and Le Deit, L., 2012, Wide distribution and glacial origin of polar gypsum on Mars: Earth and Planetary Science Letters, v. 317–318, p. 44–55, doi:10.1016/j.epsl.2011.11.035.

McEwen, A.S. et al., 2007, Mars Reconnaissance Orbiter's High Resolution Imaging Science Experiment (HiRISE): Journal of Geophysical Research, v. 112, doi:10.1029/2005JE002605.

Milana, J.P., 2009, Largest wind ripples on Earth? Geology, v. 37, p. 343–346, doi:10.1130/G25382A.1.

Nerozzi, S., and Holt, J.W., 2019, Buried Ice and Sand Caps at the North Pole of Mars: Revealing a Record of Climate Change in the Cavi Unit With SHARAD: Geophysical Research Letters, p. 2019GL082114, doi:10.1029/2019GL082114.

Pommerol, A., Appéré, T., Portyankina, G., Aye, K.-M., Thomas, N., and Hansen, C.J., 2013, Observations of the northern seasonal polar cap on Mars III: CRISM/HiRISE observations of spring sublimation: Icarus, v. 225, p. 911–922, doi:10.1016/j.icarus.2012.08.039.

Portyankina, G., Pommerol, A., Aye, K.-M., Hansen, C.J., and Thomas, N., 2013, Observations of the northern seasonal polar cap on Mars II: HiRISE photometric analysis of evolution of northern polar dunes in spring: Icarus, v. 225, p. 898–910, doi:10.1016/j.icarus.2012.10.017.

Putzig, N.E., Mellon, M.T., Herkenhoff, K.E., Phillips, R.J., Davis, B.J., Ewer, K.J., and Bowers, L.M., 2014, Thermal behavior and ice-table depth within the north polar erg of Mars: Third Planetary Dunes Systems, v. 230, p. 64–76, doi:10.1016/j.icarus.2013.07.010.

Sakamoto-Arnold, C.M., 1981a, Eolian Features Produced by the December 1977 Windstorm, Southern San Joaquin Valley, California: The Journal of Geology, v. 89, p. 129–137, doi:10.1086/628568.

Sakamoto-Arnold, C.M., 1981b, Eolian Features Produced by the December 1977 Windstorm, Southern San Joaquin Valley, California: The Journal of Geology, v. 89, p. 129–137, doi:10.1525/sp.2007.54.1.23.

Schatz, V., Tsoar, H., Edgett, K.S., Parteli, E.J.R., and Herrmann, H.J., 2006, Evidence for indurated sand dunes in the Martian north polar region: Journal of Geophysical Research, v. 111, doi:10.1029/2005JE002514.

Silvestro, S., Chojnacki, M., Vaz, D.A., Cardinale, M., Yizhaq, H., and Esposito, F., 2020, Megaripple Migration on Mars: Journal of Geophysical Research: Planets, doi:10.1029/2020JE006446.

Silvestro, S., Fenton, L.K., Vaz, D.A., Bridges, N.T., and Ori, G.G., 2010, Ripple migration and dune activity on Mars: Evidence for dynamic wind processes: Geophys. Res. Lett., v. 37, p. L20203.

Silvestro, S., Vaz, D.A., Yizhaq, H., and Esposito, F., 2016, Dune-like dynamic of Martian Aeolian large ripples: LONGITUDINAL LARGE RIPPLES ON MARS: Geophysical Research Letters, v. 43, p. 8384–8389, doi:10.1002/2016GL070014.

Smith, I.B. et al., 2018, 6th international conference on Mars polar science and exploration: Conference summary and five top questions: Icarus, v. 308, p. 2–14, doi:10.1016/j.icarus.2017.06.027.

Smith, I.B., and Holt, J.W., 2010, Onset and migration of spiral troughs on Mars revealed by orbital radar: Nature, v. 465, p. 450–453, doi:10.1038/nature09049.

Smith, I.B., and Spiga, A., 2018, Seasonal variability in winds in the north polar region of Mars: Icarus, v. 308, p. 188–196, doi:10.1016/j.icarus.2017.10.005.

Sullivan, R. et al., 2005, Aeolian processes at the Mars Exploration Rover Meridiani Planum landing site: Nature, v. 436, p. 58–61, doi:10.1038/nature03641.

Sullivan, R. et al., 2008, Wind-driven particle mobility on Mars: Insights from Mars Exploration Rover observations at “El Dorado” and surroundings at Gusev Crater: Journal of Geophysical Research, v. 113, doi:10.1029/2008JE003101.

Sullivan, R., and Kok, J.F., 2017, Aeolian Saltation on Mars at Low Wind Speeds: Low Speed Aeolian Saltation on Mars: Journal of Geophysical Research: Planets, doi:10.1002/2017JE005275.

Sullivan, R., Kok, J.F., Katra, I., and Yizhaq, H., 2020, A Broad Continuum of Aeolian Impact Ripple Morphologies on Mars is Enabled by Low Wind Dynamic Pressures: Journal of Geophysical Research: Planets, v. 125, doi:10.1029/2020JE006485.

Tanaka, K., Rodriguez, J., Skinnerjr, J., Bourke, M., Fortezzo, C., Herkenhoff, K., Kolb, E., and Okubo, C., 2008, North polar region of Mars: Advances in stratigraphy, structure, and erosional modification: Icarus, v. 196, p. 318–358, doi:10.1016/j.icarus.2008.01.021.

Urso, A., Chojnacki, M., and Vaz, D.A., 2018, Dune-Yardang Interactions in Becquerel Crater, Mars: Dune-Yardang Interactions in Becquerel Crater, Mars: Journal of Geophysical Research: Planets, doi:10.1002/2017JE005465.

Vaz, D.A., Silvestro, S., Sarmento, P.T.K., and Cardinale, M., 2017, Migrating meter-scale bedforms on Martian dark dunes: Are terrestrial aeolian ripples good analogues? Aeolian Research, v. 26, p. 101–116, doi:10.1016/j.aeolia.2016.08.003.

Wang, H., and Fisher, J.A., 2009, North polar frontal clouds and dust storms on Mars during spring and summer: Icarus, v. 204, p. 103–113, doi:10.1016/j.icarus.2009.05.028.

Wilson, I.G., 1973, Ergs: Sedimentary Geology, v. 10, p. 77–106, doi:10.1016/0037-0738(73)90001-8.

Wilson, S.A., and Zimbelman, J.R., 2004, Latitude-dependent nature and physical characteristics of transverse aeolian ridges on Mars: Journal of Geophysical Research, v. 109, doi:10.1029/2004JE002247.

Yizhaq, H., Bel, G., Silvestro, S., Elperin, T., Kok, J.F., Cardinale, M., Provenzale, A., and Katra, I., 2019, The origin of the transverse instability of aeolian megaripples: Earth and Planetary Science Letters, v. 512, p. 59–70, doi:10.1016/j.epsl.2019.01.025.

Yizhaq, H., Katra, I., Kok, J.F., and Isenberg, O., 2012, Transverse instability of megaripples: Geology, v. 40, p. 459–462, doi:10.1130/G32995.1.

Zimbelman, J.R., Irwin, R.P., Williams, S.H., Bunch, F., Valdez, A., and Stevens, S., 2009, The rate of granule ripple movement on Earth and Mars: Icarus, v. 203, p. 71–76, doi:10.1016/j.icarus.2009.03.033.

Journal of Geophysical Research – Planets

Supporting Information for

Widespread Megaripple Activity Across the North Polar Ergs of Mars

Matthew Chojnacki*[1] (mchojnacki@psi.edu), David A. Vaz[2], Simone Silvestro[3,4], and & David C.A. Silva[2].

[1]Planetary Science Institute, Lakewood, CO, USA., [2]Centre for Earth and Space Research of the University of Coimbra, Observatório Geofísico e Astronómico da Universidade de Coimbra, Coimbra, Portugal. [3]SETI Institute, Carl Sagan Center, Mountain View, CA, USA. [4]INAF Osservatorio Astronomico di Capodimonte, Napoli, Italia. *Corresponding Author

Contents of this file

Text S1-S2
Supplemental tables: Table S1-S2
Supplemental figure: Fig. S1-S6
Supplemental animations captions: Animation S1-S9
Supplementary bibliography

Introduction

Supplementary materials include a detailed methodology for the derivation of dune topography (**Section 1)** and change detection (**Section 2**). Additionally it includes tables with information for study sites (**Table S1**) and Objective 1 survey results (**Table S2**). Six supplementary figures provide additional context and details for our analysis.

Included animations provide additional evidence for bedform activity or inactivity. Animations 1-2, 4, and 6-8 were built using in-house software, which takes orthophoto subsets, stacks them in chronological order, and provides relevant context information such as Mars date (Mars year, L_s), the direction of north, and solar azimuth. As per convention, the solar longitude (L_s) range of 0°–360° defines a MY and 11 April 1955 (L_s =0°) is the start of the Mars calendar at MY01 (see *Piqueux et al.* (2015) for details). Other animations were generated from manually triangulated orthoimage subsets (see **Table S1**), and constructed in Photoshop. Compare with similar animated GIFs of non-polar migrating dunes and megaripples at http://www.uahirise.org/sim/ and some of our earlier work (Chojnacki et al., 2019; Silvestro et al., 2020).

Section 1. Derivation of dune topography and change detection

To quantify dune heights and movement, high-resolution topography and orthoimages were derived using stereo photogrammetry via SOCET SET® BAE system software (see Kirk et al., 2008). The resulting DTMs possess a horizontal post spacing of 1 meter, where the quality of pixel matching is provided by SOCET SET as a RMS error that is typically 0.3–0.7 of the HiRISE pixel scale (i.e., 25 cm) (Kirk et al., 2008; Sutton et al., 2015) and are reported in those Planetary Data Systems products (available at: https://www.uahirise.org/dtm/). These HiRISE Digital Terrain Models (DTMs) were registered to Mars Orbiter Laser Altimeter (MOLA) (Smith et al., 2001) shot points for absolute elevation. DTMs generally possess a vertical precision of ~30 cm based on the convergence angle and spatial resolution of the stereo pair (Kirk et al., 2003) and can resolve small topography such as megaripples (e.g., **Fig. S3**). Terrain artifacts generated during the photogrammetric terrain generation due to bland or deeply shadowed areas were recognized and avoided in co-registered HiRISE Figure of Merit (FOM) maps (Mattson et al., 2012). Stereo and monitoring images were then orthorectified to the DTM to allow change detection and bedform displacement quantification to be made. In some cases more recent HiRISE images were added to preexisting DTM projects (using the same quality standards) to extend the temporal coverage. DTMs available at: https://www.uahirise.org/dtm/

Section 2. Bedform sand flux calculations
Objective 3's quantification of whole dune field fluxes required multiple approaches applied to an Olympia Cavi reentrant aeolian site (232.9°E; 84.0°N). Dune slipface toe lines were mapped in QGIS at two different times (T1 and T2). These are used to derive migration vectors (m/Earth-year), assuming local bi-orthogonal trend along the lines. The heigh of the slipface is computed automatically, by sampling the image albedo and elevation along profiles which extend from the migration vectors. These two parameters are combined to allow the automatic mapping of the slipface brink points (see Fig. 3 in Urso et al. (2018)). With this procedure we estimate the volume of mobilized sediment, quantifying the fluxes ($m^3\,m^{-1}\,yr^{-1}$) continuously along the slipface. Flux uncertainties are estimated through error propagation, assuming 0.5 m of uncertainty for the displacements and slipface heights.

Many previous studies focused on barchan and barchanoid dunes, mapping dune advancement and crest height at the perceived center of the slipfaces (Bridges et al., 2011; Runyon et al., 2017; Chojnacki et al., 2017, 2019; Davis et al., 2020). Sediment fluxes were calculated multiplying the migration rate by dune height (Ould Ahmedou et al., 2007). Note that in this case, the computed fluxes correspond to discrete maximum fluxes (at the tallest section of the dune) and a likely overestimation. Instead, with the method used in this work we obtain a continuous averaged representation of the fluxes, which is more independent of the type and shape of the dunes. Thus, the adopted technique produces a more detailed representation of the avalanching fluxes, even when complex or compound slipfaces are analyzed.

Caution should be taken when comparing the results of the two methods, since fluxes can differ by one order of magnitude. Instead of reporting peak fluxes (multiplying the maximum height by the average migration, like in Urso et al. (2018)) we compute mean and median fluxes by multiplying the two variable parameters along the slipfaces. This generates lower average fluxes, yet it is a more accurate representation of the overall fluxes (the same approach was followed in the flux comparison presented by Silvestro et al. (2020). For example, at Nili Fossae Chojnacki et al. (2018) derived 7.2 ± 3.9 $m^3 m^{-1} yr^{-1}$ for whole dune fluxes (HiRISE over 5 MY) whereas Silvestro et al. (2020) derived 3.4 ± 2.2 $m^3 m^{-1} yr^{-1}$ (HiRISE over the same time period) using this technique.

Ripple and megaripple displacements were quantified for the Buzzel site using COSI-Corr. HiRISE orthoimages can present small misalignments between the CCD channels as well as long-wavelength geometric distortions caused by jitter. These will generate residual displacements that can be filtered and subtracted from COSI-Corr EW and NS displacement components (**Fig. S6**). We applied the same technique used in Silvestro et al. (2020), which applies low-pass filtering to the residual components in the bedrock areas (assuming that displacements are zero) and extrapolating the residual values to dune areas using an inpainting algorithm. The average magnitude of the residuals is low (0.3±0.1 m for the example in **Fig. S6**), attesting the accuracy of the measured displacements.

Supplemental Figures

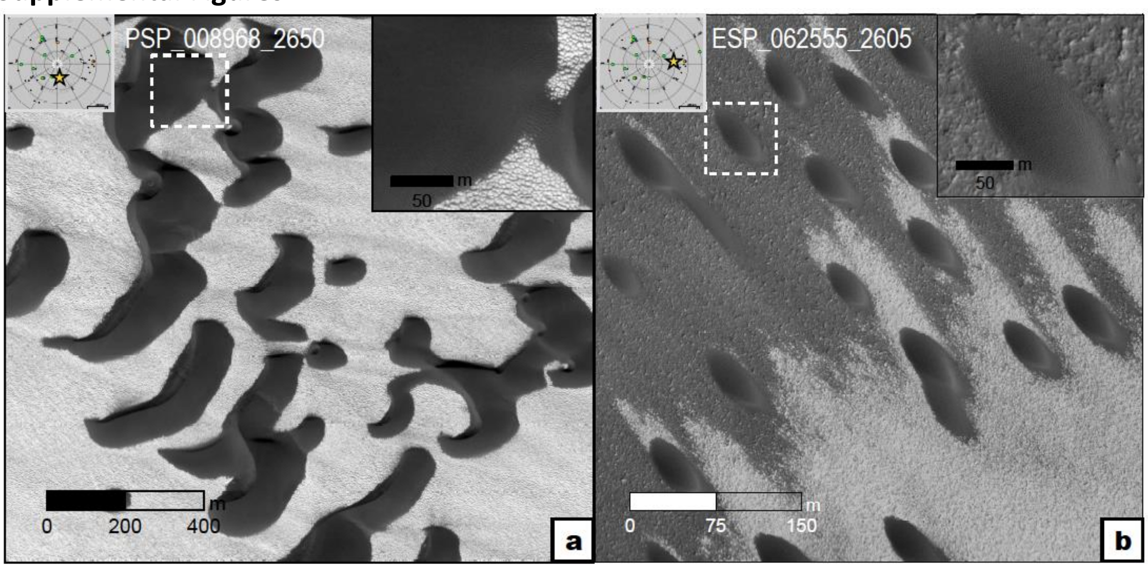

Figure S1. Two erg locations of highly active DTRs and dunes that lack intermediate-scale bedforms of either TARs or megaripples. Both locals show widely-separated dome or barchan dunes, with low sand supply conditions, and driven by broadly uni-directional winds. (a) Chasma Boreale (dune field 0010+846). (b) Olympia Cavi (dune field 0964+804). Notice the order of magnitude larger dune sizes of (a).

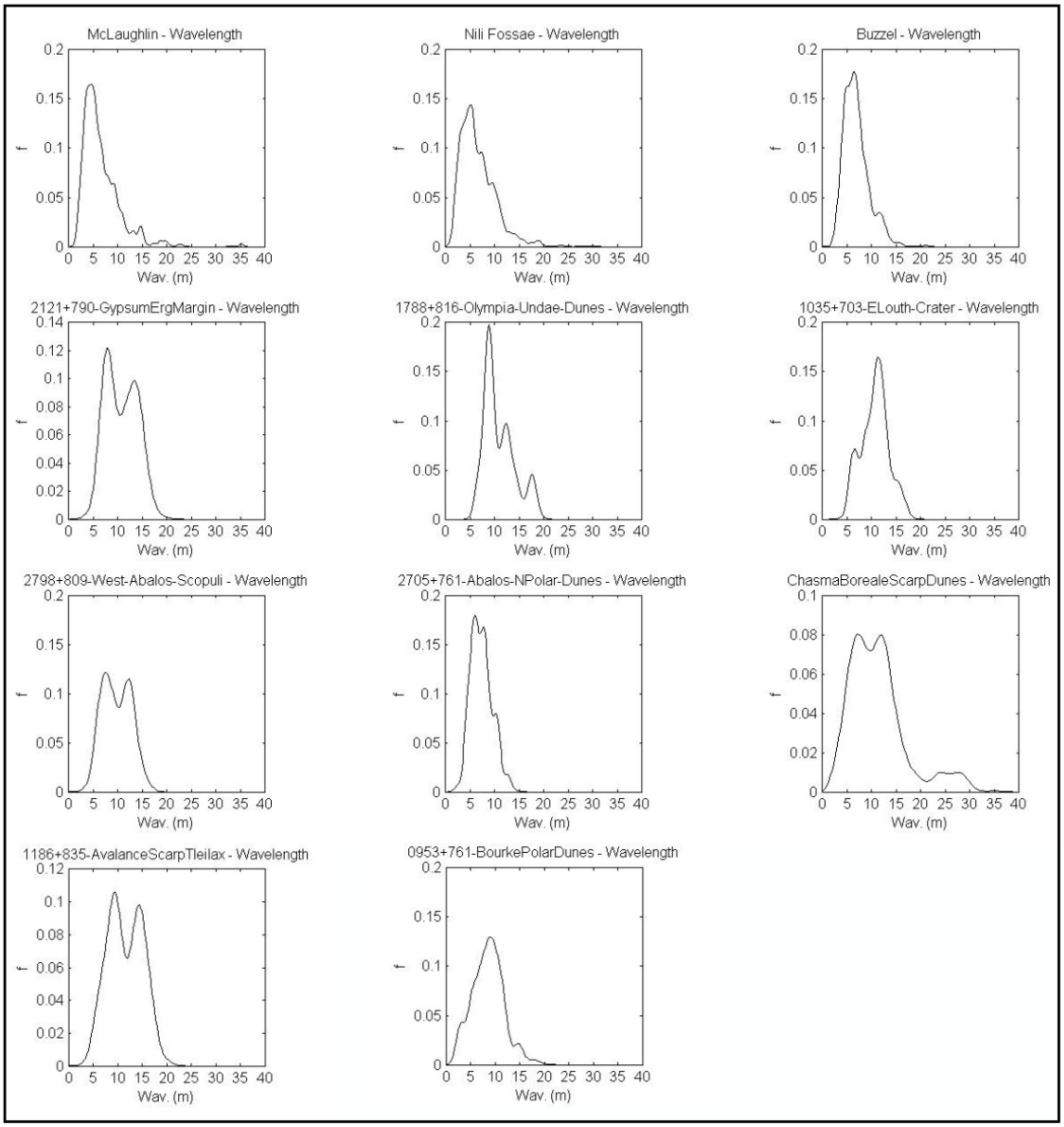

Figure S2. Histograms of active polar megaripple wavelengths from the manual mapping of crest lines. For comparison the top left and center plots are from McLaughlin/Nili Fossae (Silvestro et al., 2020). Compare with Fig 5.

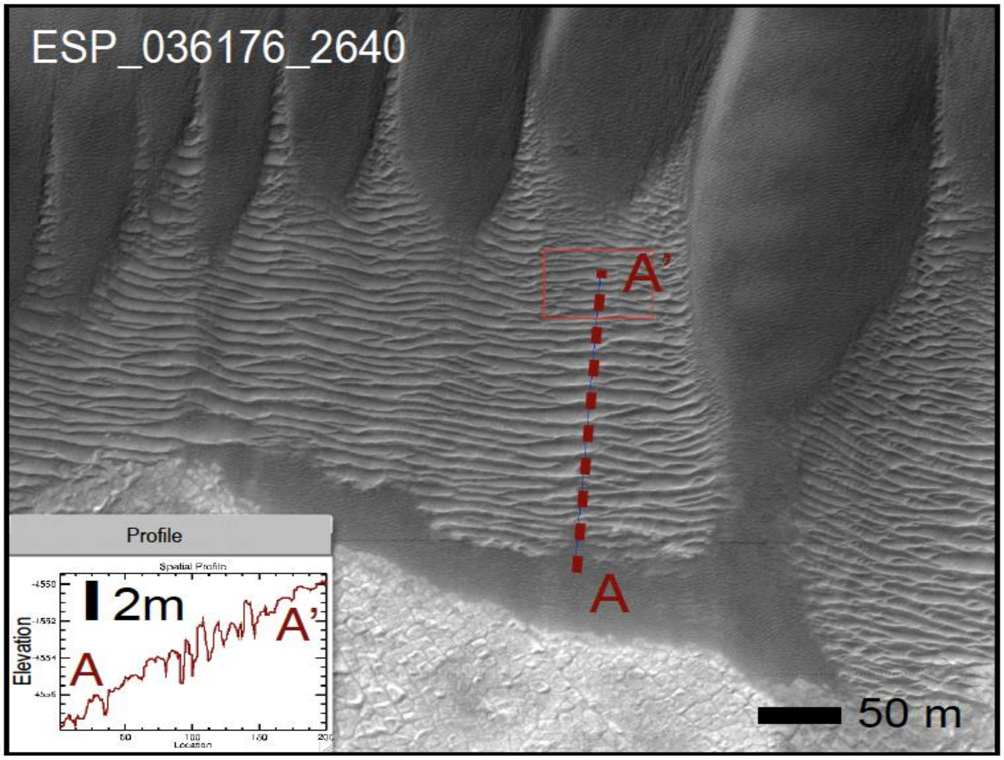

Figure S3. Example of north polar erg active megaripples where bedform heights of 1-2 m are measurable in HiRISE DTMs (1 m/post). Buzzel dune field in the Olympia Cavi reentrant.

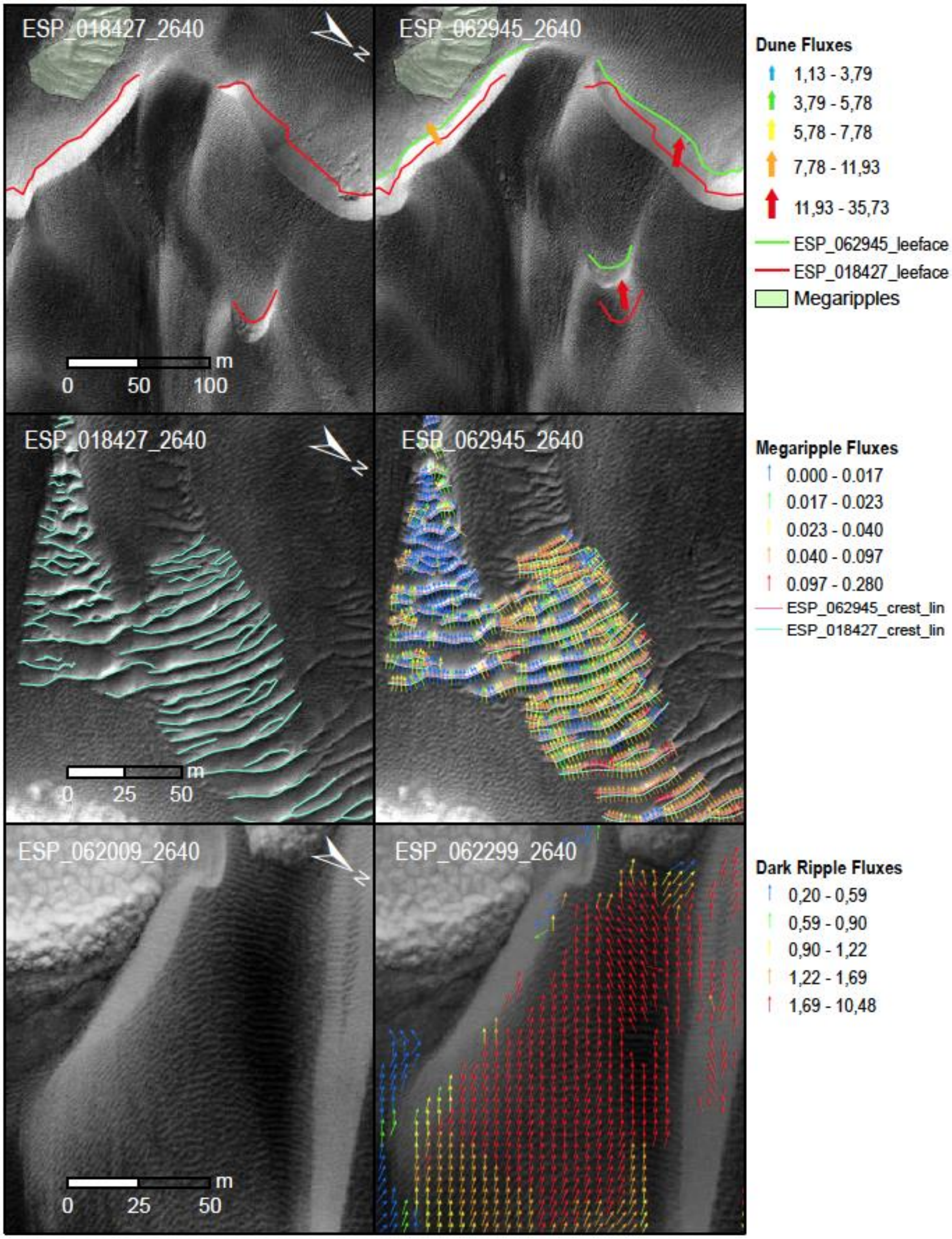

Figure S4. Examples of Buzzel bedforms measurements and activity, with (top) dune crest advancements, (middle) manually-mapped megaripple crest lines, and (bottom) ripple migration during the early summer. All comparisons show the two time periods for the same area and the right subfigures provide flux information. Compare with Fig 7. North is up in all figures.

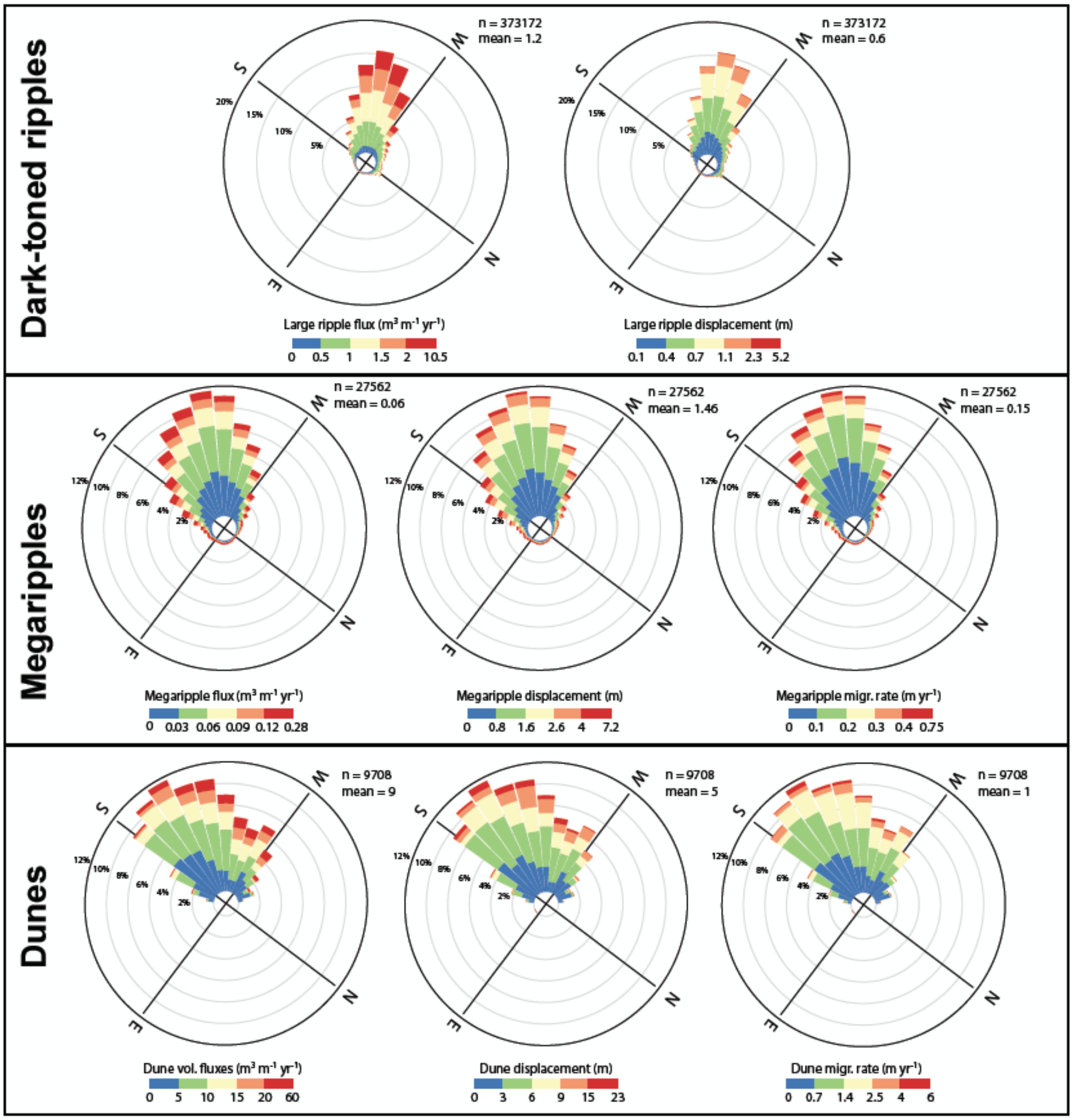

Figure S5. Circular plots showing the distribution of the Buzzel dune field DTR, megaripple, and dune (left) sand fluxes, (center) displacement, and (right) migration rate vectors. Note, ripple migration rate plot is not provided. Compare with Fig 7d.

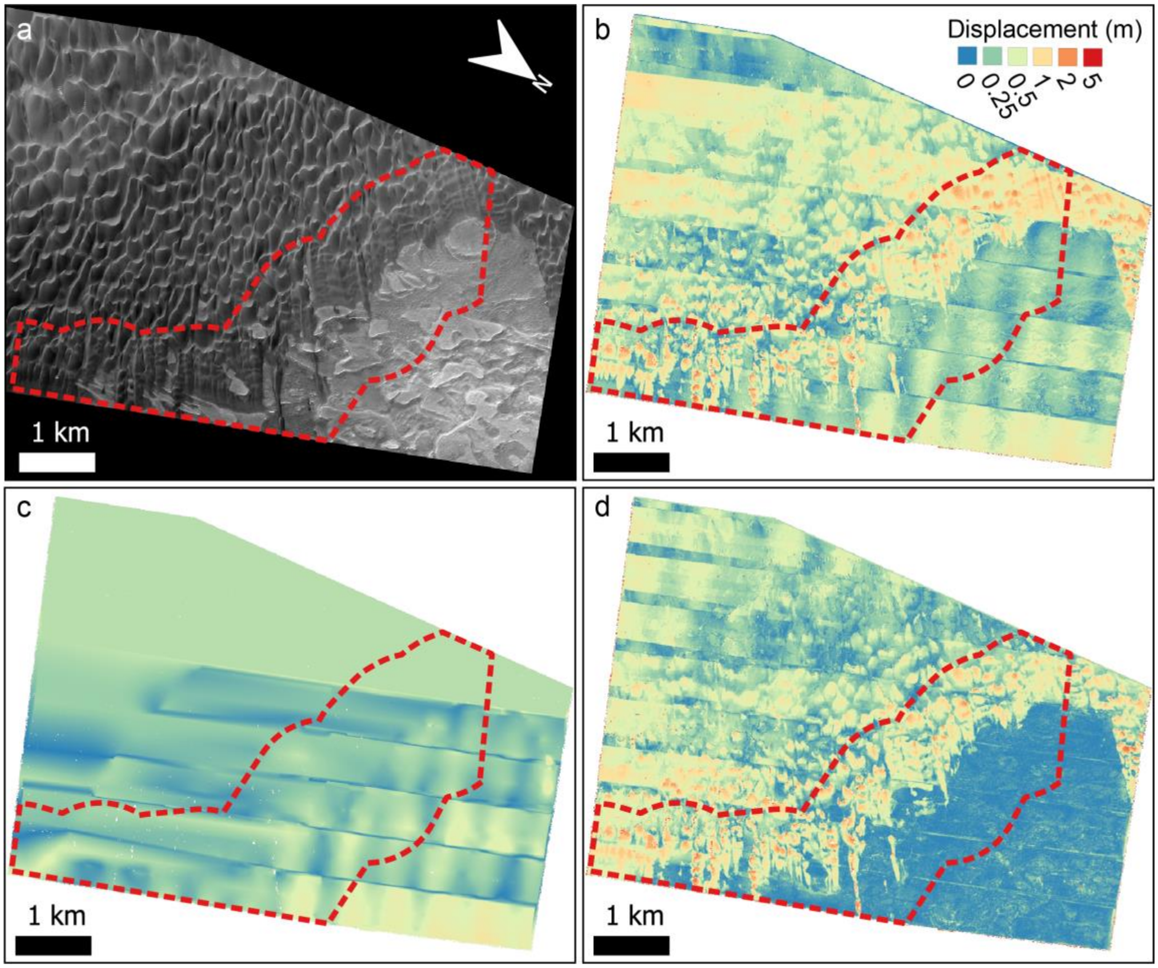

Figure S6. Example of the COSI-Corr correction that was applied to improve the bedform migration rates estimates. The red outline marks the buffer area where the fluxes of the different bedforms where compared. (a) HiRISE orthoimage ESP_062009_2640. (b) COSI-Corr displacement map used to monitor DTRs migration. Note the ~EW bands and long-wavelength wavy pattern caused by CCD misalignments and jitter. This pattern is more obvious in the bedrock areas where displacements should be null. (c) Residual displacements computed using the filtered EW and NS components (refer to Silvestro, et al. 2020 for details); the residuals are computed and extrapolated from the bedrock areas, resulting in a less effective correction with increasing distance from the dune edge. (d) The corrected displacement map; note the improvements in the dune edge, while strong banding is still visible in the southern (left) inner section of the dune field.

Supplemental Tables

Table S1. Objectives 1&2 survey results of north polar dune field morphology and activity[a].

Site name & ID	Survey status (Obj. 1)	Activity status (Obj. 2)	T1 and T2 Images and timing	Duration (Mars years)	Megaripple (MR) activity notes
Chasma Boreale Scarp Dunes - 3393+850	MR	significant megaripple migration/change	PSP_001374_2650 @Ls134 (2006) - ESP_054013_2650 @Ls124 (2018)	6.0	Many stoss and interdune MR migration. Most active MR in high sand volume fields but some on bedrock. Other static MRs in troughs or on stoss-side in the N (maybe frozen crests and/or limited upwind sand supply).
Kolhar Dunes in Chasma Boreale - 0010+846	Neither	no MRs/TARs	PSP_008968_2650 @Ls90 (2008) - ESP_063323_2650 @Ls143 (2020)	6.1	Lack of MR anywhere. Barchan and barchanoid megadunes migrating.
Buzzel Dunes and Polar Scarp - 2329+840	Both	significant megaripple migration/change	PSP_009105_2640 @Ls95 (2008) - ESP_062009_2640 @Ls94 (2019)	6.0	Most stoss leading edge MR moving; some motionless in deep troughs. Most MR in high sand volume fields but some on bedrock migrating.
Tleilax Dunes and Polar Basal Unit - 1188+834	MR	significant megaripple migration/change	PSP_001712_2635 @Ls147 (2006) - ESP_053270_2635 @Ls98 (2017)	6.2	Multiple groups of interdune MR migrating. Few stoss or cliff areas with MRs. Some motionless in deep troughs. Most MR in high sand volume fields.
Chasma Boreale Mega Dunes - 3155+826	MR	significant megaripple migration/change	ESP_027589_2630 @Ls125 (2012) - ESP_063351_2630 @Ls144 (2020)	4.2	Isolated clusters of interdune MR migrating. Truncated with short lengths. Underlying aeolian strata has static crescentic ridges.
Olympia Undae Erg Dunes - 1786+816	MR	limited migration/clear modification	ESP_019023_2620 @Ls134 (2010) - ESP_062631_2620 @Ls117 (2019)	3.9	Isolated groups of interdune MR migrating. Some motionless in deep troughs.

West Abalos Scopuli scarp layers - 2797+808	MR	significant megaripple migration/change	PSP_009433_2610 @Ls106 (2008) - ESP_062034_2610 @Ls96 (2019)	6.0	Swift DTRs near active source scarp. Upwind MR static except inter-crest sand. Upwind barchans with stoss-side migrating MRs. Static deep trough MRs.
Planum Boreum Olympia Undae dunes - 0964+804	Neither	no MRs/TARs	PSP_010020_2605 @Ls127 (2008) - ESP_062937_2605 @Ls128 (2019)	6.0	Lack of MR anywhere. Dome and barchan dunes migrating.
Polar gypsum erg margin changes - 2121+790	MR	significant megaripple migration/change	PSP_009396_2590 @Ls105 (2008) - ESP_044973_2590 @Ls116 (2016)	6.0	Skinny, bright MRs migrating on stoss side of dune and interdune MR trains. Some flank modification of MRs or static deep trough MRs.
Scandia Cavi edge linear dunes - 2094+780	MR	significant megaripple migration/change	PSP_009739_2580 @Ls117 (2008) - ESP_062551_2580 @Ls114 (2019)	6.0	Skinny, bright MRs migrating in trains on flanks of linear dunes. Other clusters of dark MR on stoss sides of dunes.
Abalos Undae Polar crater dunes - 2705+762	MR	significant megaripple migration/change	PSP_009394_2565 @Ls105 (2008) - ESP_062351_2565 @Ls107(2019)	6.0	Widespread active MRs in various contexts (extra- and intra-crater): edges of field, stoss and less sides of barchanoid, and sandsheets on steep crater walls. Isolated and as fields.
Palma (Bourke) Polar Dunes - 0953+761	MR	significant megaripple migration/change	PSP_009743_2565 @Ls117 (2008) - ESP_053469_2565 @Ls105(2017)	5.0	Clear MR migration. Mostly on stoss-side of barchanoid-pairs, none on barchans/domes. Many bright-toned MRs.
East Louth crater - 1035+703	MR	significant megaripple migration/change	PSP_001700_2505 @Ls146 (2006) - ESP_062265_2505 @Ls104 (2019)	6.9	Major changes in MR near dark dunes. Large MR. Mostly transverse motion, but some oblique. Some displacement

				on frosted MR in PSP. Less on edges of small DF.

[a]See Table 1, Fig. 2, 5 & S2 for quantitative details.

Table S2. Survey results for megaripples and TARs using HiRISE (Objective 1)[a].

Bedform class	Megaripples	TARs	Both	Neither
North Polar - 67 aeolian sites (65°N – 85°N)				
Count	59	6	6	8
Perc.	88.1%	9.0%	9.0%	11.9%
Global - 238 aeolian sites (73°S – 85°N)[b]				
Count	184	125	98	27
Perc.	77.3%	52.5%	41.2%	11.3%

[a]Also see Fig. 2 & 4.
[b]See Chojnacki et al. (2021).

Animation Captions:
Animations also available at:
https://www.dropbox.com/sh/ikzgayvdt1m9lsw/AAAZO_E3gLwY_MP7gtyOOXe7a?dl=0

Animation S1. S1_HighFluxBuzzel_animated_RED_018427-062945_2640_ULX30000_ULY26115.gif High flux dune field termed Buzzel below a NPLD scarp and sand source. Megaripples migration occurs on bedrock (lower left) and on the flank areas of proto dunes or barchans. The larger megaripple fields, while partially static, shows certain bifurcating crests that displace. Megaripples are spaced at 5-15 m. Dune field 2329+840.

Animation S2. S2_animated_RED_001374-054013_2650_ULX19621_ULY37886_b.gif Chasma Boreale scarp dunes with active megaripples (white arrows) which are more "typical" in morphology along with larger diagonal and crescentic ripples (black arrows) that show some interesting behavior. Also some long baseline slip face calving events. Dune field 3393+850.

Animation S3. S3_BedrockBuzzel.gif Megaripples migration occurs on bedrock (lower left) and on the flank areas of proto dunes or barchans. The larger megaripple fields, while partially static, shows certain bifurcating crests that displace. Megaripples are spaced at 5-15 m. Dune field 2329+840.

Animation S4. S4_animated_RED_009739-062551_2580_ULX37237_ULY34682.gif Relatively thin, bright megaripples in Scandia Cavi. Active (white arrows) and static (black) megaripples are located here. Dune field 2095+780.

Animation S5. S5_2798+809_West_Abalos_Scopuli_Untitled_009433_053805_2610.gif

An animated time-step sequence of megaripple fields as the stoss end of a west Abalos Scopuli dune field. Active (white arrows) and static (left part of sequence) megaripples are located here. Dune field 2798+809.

Animation S6. S4_BurriedBuzzel_animated_RED_009105-062299_2640_ULX59967_ULY21071_b.gif Another part of the Buzzel dune field using multiple Mars years of observations where scattered groups of megaripples are migrating. Several groups can be found overtaken and buried by ripples, sand sheets or dunes. See Animation S7 for a closer view. Note some pixel quantization occurred during image contrast matching.

Animation S7. S7_LPSC_BurriedBuzzel.gif A closer view of Buzzel dunes and sand sheets that bury megaripples over 6 Mars years. Other megaripples form or are exposed as swifter bedforms pass downwind. Scene is ~260-m-wide. See S6 for context.

Animation S8. S8_animated_RED_001374-054013_2650_ULX6528_ULY29751_b.gif Same dune field as in S2 where there are active megaripples (white arrows) along with the more frequent, brighter, long-wavelength (5-30 m) megaripple or polar TARs (black arrows) that are largely static. Note the sand pathways of proto-dunes migrating right-to-left atop of these degraded bedforms seemingly without effect (bottom two white arrows) and they are hinting that they are partially ice-cemented.

Animation S9. S9_animated_3MY_Buzzel_C.gif An animated three time-step sequence of the Buzzel dune field using 1-m/pixel orthos providing a wide-field of view. Images are spanning 3.8 and 5.7 EY. Note the upwind swift duneforms as compared with the slower barchans and megaripples. Also see Fig. 6c.

References:

Bridges, N.T. et al., 2011, Planet-wide sand motion on Mars: Geology, v. 40, p. 31–34, doi:10.1130/G32373.1.

Chojnacki, M., Banks, M.E., Fenton, L.K., and Urso, A.C., 2019, Boundary condition controls on the high-sand-flux regions of Mars: Geology, doi:10.1130/G45793.1.

Chojnacki, M., Banks, M., and Urso, A., 2018, Wind-Driven Erosion and Exposure Potential at Mars 2020 Rover Candidate-Landing Sites: Journal of Geophysical Research: Planets, v. 123, p. 468–488, doi:10.1002/2017JE005460.

Chojnacki, M., Urso, A.C., Fenton, L.K., and Michaels, T.I., 2017, Aeolian dune sediment flux heterogeneity in Meridiani Planum, Mars: Aeolian Research, v. 26, p. 73–88, doi:10.1016/j.aeolia.2016.07.004.

Chojnacki, M., Vaz, D.A., Silvestro, S., and Silva, D.C.A., 2021, Global Heterogeneity of

Martian Megaripples and Transverse Aeolian Ridges: Distribution and Activity, *in* 52nd Lunar and Planetary Science Conference, Houston, Lunar and Planetary Institute, p. Abstract #2524, http://www.lpi.usra.edu/meetings/lpsc2021/pdf/2524.pdf.

Davis, J.M., Grindrod, P.M., Boazman, S.J., Vermeesch, P., and Baird, T., 2020, Quantified Aeolian Dune Changes on Mars Derived From Repeat Context Camera Images: Earth and Space Science, v. 7, doi:10.1029/2019EA000874.

Kirk, R.L. et al., 2008, Ultrahigh resolution topographic mapping of Mars with MRO HiRISE stereo images: Meter-scale slopes of candidate Phoenix landing sites: Journal of Geophysical Research, v. 113, doi:10.1029/2007JE003000.

Kirk, R.L., Howington-Kraus, E., Redding, B., Galuszka, D., Hare, T.M., Archinal, B.A., Soderblom, L.A., and Barrett, J.M., 2003, High-resolution topomapping of candidate MER landing sites with Mars Orbiter Camera narrow-angle images: MER CANDIDATE LANDING SITE TOPOMAPPING: Journal of Geophysical Research: Planets, v. 108, doi:10.1029/2003JE002131.

Mattson, S., Bridges, N.T., Kirk, R.L., Howington-Kraus, E., Mogk, N., and Ojha, L., 2012, Studying Martian Dune Changes with HiRISE DTMs and Orthoimages, *in* Houston, Lunar and Planetary Institute, p. Abstract #7030, http://www.lpi.usra.edu/meetings/dunes2012/pdf/7030.pdf.

Ould Ahmedou, D., Ould Mahfoudh, A., Dupont, P., Ould El Moctar, A., Valance, A., and Rasmussen, K.R., 2007, Barchan dune mobility in Mauritania related to dune and interdune sand fluxes: Journal of Geophysical Research: Earth Surface, v. 112, p. F02016, doi:10.1029/2006JF000500.

Piqueux, S., Byrne, S., Kieffer, H.H., Titus, T.N., and Hansen, C.J., 2015, Enumeration of Mars years and seasons since the beginning of telescopic exploration: Dynamic Mars, v. 251, p. 332–338, doi:10.1016/j.icarus.2014.12.014.

Runyon, K.D., Bridges, N.T., Ayoub, F., Newman, C.E., and Quade, J.J., 2017, An integrated model for dune morphology and sand fluxes on Mars: Earth and Planetary Science Letters, v. 457, p. 204–212, doi:10.1016/j.epsl.2016.09.054.

Silvestro, S., Chojnacki, M., Vaz, D.A., Cardinale, M., Yizhaq, H., and Esposito, F., 2020, Megaripple Migration on Mars: Journal of Geophysical Research: Planets, doi:10.1029/2020JE006446.

Smith, D.E. et al., 2001, Mars Orbiter Laser Altimeter: Experiment summary after the first year of global mapping of Mars: J. Geophys. Res., v. 106, p. 23689–23722, doi:10.1029/2000JE001364.

Sutton, S., Chojnacki, M., Kilgallon, A., and Team, H., 2015, Precision and Accuracy of Simultaneously Collected HiRISE Digital Terrain Models, *in* 46th Lunar and Planetary Science Conference, Houston, Lunar and Planetary Institute, p. Abstract

#3010, http://www.lpi.usra.edu/meetings/lpsc2015/pdf/3010.pdf.

Urso, A., Chojnacki, M., and Vaz, D.A., 2018, Dune-Yardang Interactions in Becquerel Crater, Mars: Dune-Yardang Interactions in Becquerel Crater, Mars: Journal of Geophysical Research: Planets, doi:10.1002/2017JE005465.